Mechanisms of Inter- and Intramolecular Communication in GPCRs and G Proteins

ARTICLE *in* JOURNAL OF THE AMERICAN CHEMICAL SOCIETY · MAY 2008

Impact Factor: 12.11 · DOI: 10.1021/ja077268b · Source: PubMed

J|A|C|S
ARTICLES
Published on Web 03/12/2008

Mechanisms of Inter- and Intramolecular Communication in GPCRs and G Proteins

Francesco Raimondi,[†,‡] Michele Seeber,[†,‡] Pier G. De Benedetti,[‡] and Francesca Fanelli*[,†,‡]

Dulbecco Telethon Institute (DTI), and Department of Chemistry, University of Modena and Reggio Emilia, via Campi 183, 41100 Modena, Italy

Received September 19, 2007; E-mail: fanelli@unimo.it

Abstract: This study represents the first attempt to couple, by computational experiments, the mechanisms of intramolecular and intermolecular communication concerning a guanidine nucleotide exchange factor (GEF), the thromboxane A2 receptor (TXA_2R), and the cognate G protein (Gq) in its heterotrimeric GDP-bound state. Two-way pathways mediate the communication between the receptor−G protein interface and both the agonist binding site of the receptor and the nucleotide binding site of the G protein. The increase in solvent accessibility in the neighborhoods of the highly conserved E/DRY receptor motif, in response to agonist binding, is instrumental in favoring the penetration of the C-terminus of Gq_α in between the cytosolic ends of H3, H5, and H6. The arginine of the E/DRY motif is predicted to be an important mediator of the intramolecular and intermolecular communication involving the TXA_2R. The receptor−G protein interface is predicted to involve multiple regions from the receptor and the G protein α-subunit. However, receptor contacts with the C-terminus of the α5-helix seem to be the major players in the receptor-catalyzed motion of the α-helical domain with respect to the Ras-like domain and in the formation of a nucleotide exit route in between the αF-helix and β6/α5 loop of Gq_α. The inferences from this study are of wide interest, as they are expected to apply to the whole rhodopsin family, given also the considerable G protein promiscuity.

1. Introduction

G protein-coupled receptors (GPCRs) constitute the largest superfamily of membrane proteins known to date that act as guanine nucleotide exchange factors (GEFs) following the coupling to GDP-bound heterotrimeric intracellular G proteins. GPCRs share seven transmembrane helices bundled up to form a polar internal tunnel and expose the N-terminus and three interconnecting loops, to the exterior, and the C-terminus, with a matching number of loops, to the interior of the cell.

The G proteins consist of three subunits α, β, and γ (reviewed in refs 1−3). The α-subunits are enzymes of the Ras superfamily, which hydrolyze GTP to transduce external signals and to regulate events within cells. In the inactive state, G proteins form membrane-associated αβγ heterotrimers, with GDP tightly bound to the α-subunit. Upon activation by extracellular signals, receptors catalyze the exchange of bound GDP for GTP. The GTP-bound form of the heterotrimer is unstable and heterolytically dissociates to form active GTP-α and βγ complexes (reviewed in refs 1−3). Recent experimental evidence, however, indicate that G protein activation may be not concurrent with dissociation of α from βγ.[4,5]

Crystallographic studies of G protein α-subunits and heterotrimers provided significant insight into our understanding of how these nanomachines might work (reviewed in refs 3, 6). Structural studies of α-subunits essentially focused on Gt_α, transducin, involved in vertebrate vision (reviewed in refs 6, 7), Gi_α (reviewed in refs 6, 7) and Gs_α,[8] respectively involved in hormone-regulated inhibition and activation of adenylate cyclase. The α-subunit consists of two domains, the GTPase (Ras-like) domain, which contains a six-stranded β-sheet surrounded by six α-helices, and the helical domain, constituted by a long central helix surrounded by five shorter helices. GDP is bound into a cleft between the GTPase and the helical domains. Both domains have almost identical structures in the GTP and GDP-bound states. Significant changes are observed within the GTPase domain contacting $Gt_{\beta\gamma}$; in fact, these regions are disordered in the inactive heterotrimeric forms, whereas they are ordered in the Mg^{2+}-GTPγS-activated structures of Gt_α and Gi_α (reviewed in ref 6). The N-terminal region of the α-subunit consists of a long α-helix pointing out from the rest of the subunit. This feature was revealed by the structure of heterotrimeric Gt and Gi, as the α-helical conformation of the N-terminus is stabilized by the βγ complex, whereas such domain is disordered in the isolated α-subunits.[6,9] The last 10 amino acids of Gt_α are predicted to hold an α-helical conforma-

[†] Dulbecco Telethon Institute (DTI).
[‡] University of Modena and Reggio Emilia.

(1) Gilman, A. G. *Annu. Rev. Biochem.* **1987**, *56*, 615−49.
(2) Clapham, D. E. *Nature* **1996**, *379*, 297−9.
(3) Oldham, W. M.; Hamm, H. E. *Q. Rev. Biophys.* **2006**, *39*, 117−66.
(4) Bunemann, M.; Frank, M.; Lohse, M. J. *Proc. Natl. Acad. Sci. U.S.A.* **2003**, *100*, 16077−82.
(5) Klein, S.; Reuveni, H.; Levitzki, A. *Proc. Natl. Acad. Sci. U.S.A.* **2000**, *97*, 3219−23.
(6) Coleman, D. E.; Sprang, S. R. *Trends Biochem. Sci.* **1996**, *21*, 41−4.
(7) Bohm, A.; Gaudet, R.; Sigler, P. B. *Curr. Opin. Biotechnol.* **1997**, *8*, 480−7.
(8) Sunahara, R. K.; Tesmer, J. J.; Gilman, A. G.; Sprang, S. R. *Science* **1997**, *278*, 1943−7.

10.1021/ja077268b CCC: $40.75

tion in the rhodopsin-bound forms, whereas they appear to be disordered in the receptor-dissociated forms.[6,10,11] Very recent site-directed spin labeling (SDSL) experiments on the GDP and GTP$_\gamma$S-bound forms of Gi$_\alpha$ revealed an increase in dynamics of switch II (i.e., the domain that connects the β3-strand to the α2-helix according to the nomenclature proposed by Noel and co-workers[12] (Figure 1a)) upon receptor-induced G$_\alpha$ activation.[13]

Computational experiments on the GDP and GTPγS-bound forms of transducin revealed a number of nucleotide-dependent structural and dynamic changes not shown by the crystal structures.[14] Indeed, these experiments showed the existence of a front to back communication involving the β2-β3 hairpin, the α1-helix, and the α5-helix.[14]

The β-subunit, a member of the WD repeat family of proteins, has a long N-terminal helix followed by a repeating module of seven β-sheets, each with four antiparallel strands, forming a β-propeller structure.[3,6,7,15,16] The γ-subunit contains two helices: the N-terminal helix interacts with the N-terminal helix of β, whereas the remaining polypeptide chain of γ interacts with the β-propeller structure of β.[3,6,7,15,16] Similarly to the C-tail of the α-subunit, the C-tail of the γ chain (i.e., the (60−71)-farnesyl peptide) holds a regular α-helical structure when bound to activated rhodopsin (i.e., Meta II, MII), whereas its conformation is disordered in the receptor-dissociated forms of the $\beta\gamma$ complex.[17] Thus, *in vitro* experiments suggest that activated receptor controls the conformation of the C-tails of the G protein α- and γ-subunits.[10,11,17]

So far, inferences on the putative mechanism of receptor-catalyzed nucleotide exchange relied on low-resolution biochemical and biophysical experiments, as no high-resolution structural information is available on the active states of GPCRs or on their complexes with the cognate G proteins. The only high-resolution structural information available at the moment concerns rhodopsin, the cornerstone of family A GPCRs in its dark (inactive) state (reviewed in ref 18), and the human β2-adrenergic receptor (β2-AR)−T4 lysozyme fusion protein (at 2.4 Å resolution) bound to the partial inverse agonist carazolol.[19,20]

In contrast, atomistic information on the structural/dynamics features of the inactive and active states of the homologous GPCRs rely on computational experiments, which highlighted the release of the interactions involving the arginine of the E/DRY motif as the major structural perturbations associated with the transitions from the inactive to the active states

Figure 1. (a) Primary sequence of the mouse Gq$_\alpha$. Grey shadows and boxes indicate regions in α-helix and β-strand, respectively. Red letters indicate the amino acids involved in interaction with the WT^{U466} along the 6-ns trajectory of the best predicted complex. Bold letters and stars indicate amino acids in the GDP binding site. Noel's nomenclature is also reported. The reported length of the secondary structure elements was computed on the input structure. (b) Sequence alignment between a shortened form of bovine rhodopsin (PDB code: 1U19, i.e. template, and the human TXA$_2$R (target) that was employed for comparative modeling. The amino acid stretches 64−67, 106−108, and 279−284 were deleted from the 1U19 template. Underlined sequences in the target receptor (i.e., segments 48−55, 99−106, 268−273, and 284−291) indicate the amino acids subjected to α-helical restraints during comparative modeling. The boxed amino acid in each rhodopsin helix corresponds to the amino acid no. 50 according to the Ballesteros and Weinstein nomenclature, (see Methods) whereas the boxed amino acid stretch in both sequences at the end of H7 corresponds to H8. Red letters indicate the WT^{U466} amino acids involved in interaction with Gq$_\alpha$ along the 6-ns trajectory of the best predicted complex.

(reviewed in ref 21). In addition, our computational experiments showed the increase in the solvent accessibility of selected amino acids at the cytosolic extensions of helices (H) 3, 5, and 6 as

(9) Medkova, M.; Preininger, A. M.; Yu, N. J.; Hubbell, W. L.; Hamm, H. E. *Biochemistry* **2002**, *41*, 9962−72.
(10) Kisselev, O. G.; Kao, J.; Ponder, J. W.; Fann, Y. C.; Gautam, N.; Marshall, G. R. *Proc. Natl. Acad. Sci. U.S.A.* **1998**, *95*, 4270−5.
(11) Koenig, B. W.; Kontaxis, G.; Mitchell, D. C.; Louis, J. M.; Litman, B. J.; Bax, A. *J. Mol. Biol.* **2002**, *322*, 441−61.
(12) Noel, J. P.; Hamm, H. E.; Sigler, P. B. *Nature* **1993**, *366*, 654−663.
(13) Van, Eps, N.; Oldham, W. M.; Hamm, H. E.; Hubbell, W. L. *Proc. Natl. Acad. Sci. U.S.A.* **2006**, *103*, 16194−9.
(14) Ceruso, M. A.; Periole, X.; Weinstein, H. *J. Mol. Biol.* **2004**, *338*, 469−81.
(15) Wall, M. A.; Coleman, D. E.; Lee, E.; Iniguez-Lluhi, J. A.; Posner, B. A.; Gilman, A. G.; Sprang, S. R. *Cell* **1995**, *83*, 1047−58.
(16) Lambright, D. G.; Sondek, J.; Bohm, A.; Skiba, N. P.; Hamm, H. E.; Sigler, P. B. *Nature* **1996**, *379*, 311−9.
(17) Kisselev, O. G.; Downs, M. A. *Structure (Camb)* **2003**, *11*, 367−73.
(18) Palczewski, K. *Annu. Rev. Biochem.* **2006**, *75*, 743−67.
(19) Rosenbaum, D. M.; Cherezov, V.; Hanson, M. A.; Rasmussen, S. G.; Thian, F. S.; Kobilka, T. S.; Choi, H. J.; Yao, X. J.; Weis, W. I.; Stevens, R. C.; Kobilka, B. K. *Science* **2007**, *318*, 1266−73.
(20) Cherezov, V.; Rosenbaum, D. M.; Hanson, M. A.; Rasmussen, S. G.; Thian, F. S.; Kobilka, T. S.; Choi, H. J.; Kuhn, P.; Weis, W. I.; Kobilka, B. K.; Stevens, R. C. *Science* **2007**, *318*, 1258−65.
(21) Fanelli, F.; De Benedetti, P. G. *Chem. Rev.* **2005**, *105*, 3297−3351.

the structural change characterizing mutation- and ligand-induced receptor activation (reviewed in ref 21). These inferences are being supported by the recent release of the low-resolution structure of a photoactivated deprotonated intermediate of bovine rhodopsin, reminiscent of the G protein signaling state MII (i.e., PDB code: 2I37, 4.15 Å).[22] In fact, although it is still a matter of debate to what extent the activated structure represents the native MII state, comparisons of the dark and photoactivated structures at the same resolution (i.e., PDB codes 2I36 and 2I37, respectively)[22] show that the major differences between the two rhodopsin states consist of modest increases in the solvent accessibility of selected amino acids in the neighborhood of the E/DRY motif in the activated form compared to the inactive one. These crystallographic data, although at a low resolution, seem to be consistent with recent in vitro evidence from site directed spin labeling (SDSL)[23,24] experiments underscoring that the dramatic detachment between H3 and H6 that accompanies rhodopsin activation in detergent[25] is no longer observed in rhodopsin reconstituted in lipid bilayers. Collectively, crystallographic as well as early and more recent SDSL data suggest that differences between dark rhodopsin and MII would be larger than those shown by the crystal structures,[22] but lower than those predicted by SDSL in detergents,[25] and would include an increase in solvent accessibility in the neighborhoods of the E/DRY motif as a structural feature of the active states.

In line with inferences of computational modeling on the isolated receptors, the patchwork of the most relevant information from *in vitro* experiments on receptor−G protein recognition, in particular on the rhodopsin−transducin system, suggests that the E/DRY motif and the cytosolic extensions of H3, H5, H6, and H8 of GPCRs would recognize the α4/β6 loop and the C-terminus of Gt_α (reviewed in refs 3, 21). Consensus from in vitro experiments exists on the hypothesis that multiple G protein and receptor domains participate in the receptor−G protein interface (reviewed in refs 3, 21).

Different mechanisms of receptor-catalyzed GDP release have been proposed. According to the so-called "lever-arm" model, the β3/α2 loop of the α-subunit acts as a potential "lip" that prevents GDP release.[26,27] GPCRs are thought to use the G_α N-terminus to tilt $G_{\beta\gamma}$ away from G_α, thereby opening the β3/α2 lip. The recently released crystal structure of the GEF peptide KB-752 bound to Gi_α seems to support the "lever-arm" model.[28] Indeed, by binding between the switch II and the α3-helix, KB-752 pushes the α2-helix away from the nucleotide. Displacement of switch II results in the β3/α2 loop also being pulled away from the nucleotide in a way that might allow more efficient GDP egress. Thus, according to this model, the proposed exit route for GDP lies at the $G_\alpha-G_\beta$ interface, which becomes more accessible following the displacement of the occlusive β3/α2 loop. An alternative opinion on the mechanism of receptor-catalyzed nucleotide exchange suggests that GPCRs use the G_α N-terminus to move $G_{\beta\gamma}$ in an opposite fashion to that proposed by the "lever-arm" model.[29] According to this "gear-shift" model, $G_{\beta\gamma}$ is shifted toward G_α, resulting in a closely packing $G_\alpha-G_\beta$ interface. This $G_{\beta\gamma}$ shift is proposed to alter the conformation of the α5-helix. A different GDP exit route, as compared to the one proposed by the "lever-arm" model or inferred from the crystal structure of the KB-752−Gi_α complex, derives from site-directed mutagenesis experiments implicating the C-terminus of the α5-helix in the receptor-catalyzed GDP exchange[30,31] as well as from the results of very recent SDSL experiments on Gi_α.[32,33] The latter, indeed, identified a possible allosteric pathway propagated along switch I at the $G_\alpha-G_\beta$ interface to the αF-helix, which, like the α5-helix and the α5/β6 loop, forms part of a putative GDP exit route.[33]

Chart 1

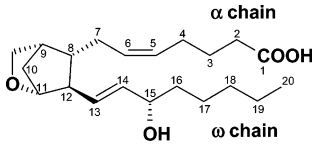

U-46619

In this study, a well-established computational approach, based upon comparative modeling, ligand-protein and protein−protein docking simulations as well as molecular dynamics (MD) simulations and analyses, has been employed to investigate the mechanism of intramolecular and intermolecular communication involving the thromboxane A_2 receptor (TXA_2R), a member of the rhodopsin family, and its cognate G protein (Gq).

For the first time, the intrinsic structural differences between inactive and ligand-induced active receptor states have been connected with the G proteins recognition properties of the receptor. In this respect, the role of the arginine of the highly conserved E/DRY motif both in receptor activation and G protein recognition has been investigated to provide insights into the results of in vitro experiments on the TXA_2R, which implicated the conserved arginine in G protein recognition rather than in receptor activation.[34] This aim has been accomplished by comparing the structural/dynamics features of the empty wild type TXA_2R (i.e., WT) with those of the agonist-bound forms of the WT (WT^{U466}) and of the R130V inactive mutant (i.e., $R130V^{U466}$),[34] characterized by the replacement of the E/DRY arginine with a valine. The U-46619 agonist shown in Chart 1 was employed to simulate the active state ensembles.

The results of this study provide significant insights into (a) the structural features of the receptor−G protein interface, (b) the G protein domains that undergo significant conformational changes in response to receptor binding, (c) the putative allosteric pathway of receptor-catalyzed nucleotide exchange,

(22) Salom, D.; Lodowski, D. T.; Stenkamp, R. E.; Le Trong, I.; Golczak, M.; Jastrzebska, B.; Harris, T.; Ballesteros, J. A.; Palczewski, K. *Proc. Natl. Acad. Sci. U.S.A* **2006**, *103*, 16123−8.
(23) Kusnetzow, A. K.; Altenbach, C.; Hubbell, W. L. *Biochemistry* **2006**, *45*, 5538−50.
(24) Park, P. S.; Lodowski, D. T.; Palczewski, K. *Annu. Rev. Pharmacol. Toxicol.* **2007**.
(25) Farrens, D. L.; Altenbach, C.; Yang, K.; Hubbell, W. L.; Khorana, H. G. *Science* **1996**, *274*, 768−70.
(26) Iiri, T.; Farfel, Z.; Bourne, H. R. *Nature* **1998**, *394*, 35−8.
(27) Rondard, P.; Iiri, T.; Srinivasan, S.; Meng, E.; Fujita, T.; Bourne, H. R. *Proc. Natl. Acad. Sci. U.S.A.* **2001**, *98*, 6150−5.
(28) Johnston, C. A.; Willard, F. S.; Jezyk, M. R.; Fredericks, Z.; Bodor, E. T.; Jones, M. B.; Blaesius, R.; Watts, V. J.; Harden, T. K.; Sondek, J.; Ramer, J. K.; Siderovski, D. P. *Structure* **2005**, *13*, 1069−80.
(29) Cherfils, J.; Chabre, M. *Trends Biochem. Sci.* **2003**, *28*, 13−7.
(30) Marin, E. P.; Krishna, A. G.; Sakmar, T. P. *J. Biol. Chem.* **2001**, *276*, 27400−5.
(31) Marin, E. P.; Krishna, A. G.; Sakmar, T. P. *Biochemistry* **2002**, *41*, 6988−94.
(32) Oldham, W. M.; Van Eps, N.; Preininger, A. M.; Hubbell, W. L.; Hamm, H. E. *Nat. Struct. Mol. Biol.* **2006**, *13*, 772−7.
(33) Oldham, W. M.; Van Eps, N.; Preininger, A. M.; Hubbell, W. L.; Hamm, H. E. *Proc. Natl. Acad. Sci. U.S.A* **2007**, *104*, 7927−32.
(34) Capra, V.; Veltri, A.; Foglia, C.; Crimaldi, L.; Habib, A.; Parenti, M.; Rovati, G. E. *Mol. Pharmacol.* **2004**, *66*, 880−9.

and (d) the G protein domains that participate in the GDP exit route.

The inferences from this study are of wide interest as they are expected to apply to the whole rhodopsin family, given also the very high G protein promiscuity.

2. Methods

2.1. Comparative Modeling of the TXA_2R. Comparative modeling of the α-isoform of the human TXA_2R was carried out by means of the software MODELER 7v7,[35] by using the most complete and highest resolved structure of rhodopsin as a template (i.e., PDB code: 1U19).[36] The whole sequence of the receptor, i.e., comprising the seven helices, the three intracellular and three extracellular loops (IL and EL, respectively), and the N- and C-termini, was modeled. The lack of homology between the template and target proteins essentially resides in IL1, EL1, and EL3, which have to be modeled following de novo approaches, like the one implemented in the MODELLER program, eventually combined with the addition of external α-helix restraints, which serve to extend the transmembrane helices bridged by these loops.[37] MODELLER is, indeed, based upon the satisfaction of stereochemical restraints, which, for the homologous regions, are transferred from the template to the target protein, whereas, for the nonconserved portions, can be added by the user or computed following an energy-based de novo protocol.[38] Thus, in our case study, in order to define the proper lengths of the nonhomologous unstructured portions, 13 different modifications of the rhodopsin template were probed, which were variably deleted at the IL1, EL1, and EL3 nonhomologous domains. Finally, eight different alignments between the target sequence and four different variances of the rhodopsin template were chosen to produce multiple models. From each alignment, 200 receptor models were achieved by randomizing the Cartesian coordinates of the model. Randomizations produced 1600 models. Finally, the models resulting from four of the eight tested alignments revealed significantly higher quality than the rest. From each set of the 200 models derived from the best four alignments one model was selected, which was characterized by the highest 3D-Profile score (as computed within the QUANTA package) among the ten models characterized by the lowest restraint violations (i.e., the lowest MODELLER Objective Function). These four different models can be divided into two pairs, each sharing a common modified rhodopsin template. In detail, one pair of models (i.e., TXA_2R_{1DISU}), obtained from the rhodopsin template shown in Figure 1b, is characterized by the presence of one disulfide bridge between C105(3.25) and C183 (in EL2), homologous to the one in rhodopsin structure and consistent with experimental evidence.[39] The numbering in parenthesis follows the scheme proposed by Ballesteros and Weinstein,[40] where the first number indicates the helix and the numbers thereafter indicate the position of the helical residue relative to the most highly conserved residue within that helix, which is denoted as 50 (boxed in Figure 1b). In contrast, the other pair of models (i.e., TXA_2R_{2DISU}), obtained from an alternative rhodopsin variance, is characterized by the presence of a disulfide bridge between C11 (in the N-terminus) and C102(3.22) in addition to the one inherited from rhodopsin structure. The additional bridge was imposed because of the suitable distance between the C11 (in the N-terminus) and C102(3.22) sulfur atoms in the target receptor models.

The results shown in this work refer to the alignment reported in Figure 1b, by employing the rhodopsin template deprived of the 64−67, 106−108, and 279−284 amino acid stretches. The employment of this rhodopsin variance was associated with the application of α-helix restraints to the 48−55, 99−106, 268−273, and 284−291 amino acid stretches of the target receptors (underlined sequences in Figure 1b). These restraints resulted in one- or two-turn elongation of the intracellular ends of H1 and of the extracellular ends of H3, H6, and H7 (Figure 1b). For selected TXA_2R models, refinements of the amino acid stretch 274−283, corresponding to EL3, were carried out by using an energy based de novo method implemented in MODELLER.[37]

The four TXA_2R models were subjected to automatic and manual rotation of the side-chain torsion angles when in nonallowed conformations, leading to three alternative combinations of side-chain rotamers for each model. The twelve models, six from the '1DISU' and six from the '2DISU' sets were used as input structures for MD simulations.

2.2. Molecular Dynamics Simulations of the Isolated Receptor Forms. MD simulations were carried out first on the WT form of the TXA_2R. In detail, the twelve TXA_2R models achieved by comparative modeling were subjected to energy minimization and MD simulations by using the GBSW implicit membrane−water model[41] recently implemented in CHARMM.[42] With respect to the physical parameters representing the membrane in the GBSW model, the surface tension coefficient (representing the nonpolar solvation energy) was set to 0.03 kcal/(mol·A^2). The membrane thickness centered at $Z = 0$ was set to 35.0 Å with a membrane smoothing length of 5.0 Å ($w_m = 2.5$ Å).

Minimizations were carried out by using 1500 steps of steepest descent followed by Adopted Basis Newton−Raphson (ABNR) minimization, until the root-mean-square gradient was less than 0.001 kcal/mol Å.

With respect to the setup of MD simulations, the lengths of the bonds involving the hydrogen atoms were restrained by the SHAKE algorithm, allowing for an integration time step of 0.001 ps. The systems were heated to 300 K with 7.5 K rises every 2.5 ps per 100 ps by randomly assigning velocities from a Gaussian distribution. After heating, the system was allowed to equilibrate for 100 ps.

For the six different TXA_2R_{1DISU} models, one disulfide bridge patch was applied to C105(3.25) and C183 (in EL2), consistent with experimental evidence,[39] whereas, for the six TXA_2R_{2DISU} models, a second disulfide bridge patch was applied to C11 (in the N-terminus) and C102(3.22).

The secondary structure of the helix bundle was preserved by assigning distance restraints (i.e., minimum and maximum allowed distances of 2.7 Å and 3.0 Å, respectively) between the backbone oxygen atom of residue i and the backbone nitrogen atom of residue i+4, except for prolines. The scaling factor of such restraints was 10 and the force constant at 300 K was 10 kcal/mol Å. The receptor amino acids present in noncanonical α-helical conformations in the input structure, a condition inherited from the rhodopsin template, were not subjected to any intrabackbone distance restraint. The selected intrahelix distance restraints were the outcome of short (100 ps) equilibrated MD trial runs, in which the beginning and ending of such restraints in each helix was varied. Trials included also reprotonation and deprotonation of D304(7.49) that, in TXA_2R, substitutes for the highly conserved asparagine of the NPxxY motif. The selected computational setup was employed to produce 1 ns equilibrated trajectories for each of the 12 different receptor input structures. The selected setup comprised also D304(7.49) in the reprotonated (neutral) state. The rational for choosing the neutral state of D7.49 is that it produced a lower deviation between simulated model and crystal structure of rhodopsin, consistent with the fact that the neutralized aspartate is a better mimic of the highly conserved asparagine.

Finally, the trajectory that produced an average arrangement, which retained at best the structural features inherited from rhodopsin structure and which was the best representative of all the other trajectories, was

(35) Sali, A.; Blundell, T. L. *J. Mol. Biol.* **1993**, *234*, 779−815.
(36) Okada, T.; Sugihara, M.; Bondar, A. N.; Elstner, M.; Entel, P.; Buss, V. *J. Mol. Biol.* **2004**, *342*, 571−83.
(37) Fiser, A.; Do, R. K.; Sali, A. *Protein Sci.* **2000**, *9*, 1753−73.
(38) Marti-Renom, M. A.; Stuart, A.; Fiser, A.; Sánchez, R.; Melo, F.; Sali, A. *Annu. Rev. Biophys. Biomol. Struct.* **2000**, *29*, 291−325.
(39) D'Angelo, D. D.; Eubank, J. J.; Davis, M. G.; Dorn, G. W., 2nd *J. Biol. Chem.* **1996**, *271*, 6233−40.
(40) Ballesteros, J. A.; Weinstein, H. *Methods Neurosci.* **1995**, *25*, 366−428.
(41) Im, W.; Feig, M.; Brooks, C. L., III *Biophys. J.* **2003**, *85*, 2900−18.
(42) Brooks, B. R.; Bruccoleri, R. E.; Olafson, B. D.; States, D. J.; Swaminathan, S.; Karplus, M. *J. Comput. Chem.* **1983**, *4*, 187−217.

prolonged to 4 ns. Such a selected trajectory involved an input structure from the $TXA2R_{1DISU}$ set of models. That input structure and the computation conditions that originated the selected trajectory were used to produce the WT^{U466} and $R130V^{U466}$ complexes. In this respect, the structural model of the U-46619 agonist (Chart 1) was built by means of the QUANTA2005 package. The stereochemistry of the bonds connecting the α and ω chains to the cyclopentane ring as well as that of the double bonds was set similar to that in the crystal structure of TXB_2.[43,44] The optimized geometry and charge distribution of the ligand were computed through semiempirical MO calculations (AM1).[45] The agonist was, hence, manually docked into the selected input structure of the WT receptor. The key interactions considered for driving the initial orientation of U-46619 into the binding site of TXA_2R were the charge reinforced H-bond between R295(7.40) and the carboxylate of the ligand, as well as the H-bond between S201(5.43) and the hydroxy group of the ligand, according to experimental evidence.[46,47] The establishment of these interactions impedes the formation of the intramolecular H-bond between the α and ω chains of the agonist, as inferred from spectroscopic measurements.[43] In agreement with experimental evidence,[48] the accomplishment of the two intermolecular H-bonds implies the involvement of EL2 in contacts with the agonist. Eighteen 1 ns MD runs were carried out on eight different agonist−receptor complexes by probing different intermolecular distance restraints between the hydroxy groups of the agonist and of S201(5.43). Finally, the input complex and intermolecular distance restraints that accomplished the best agonist−receptor complementarity were used to produce the complex of the R130V mutant by introducing the amino acid substitution at the 3.50 site. Four-nanosecond equilibrated trajectories were, hence, produced for the selected complexes of WT^{U466} and $R130V^{U466}$. The selected interoxygen distance restraints consisted in a minimum and maximum allowed distances of 2.5 Å and 2.9 Å, respectively. To give more strength to the inferences from MD analysis, agonist−receptor complexes were built by also employing one of the alternative receptor models belonging to the TXA_2R_{2DISU} set. Also in this case, eighteen parallel 1 ns MD simulations were carried out differing in the input orientation and conformation of the agonist and the binding-site amino acids as well as in the intermolecular distance restraints between the hydroxy oxygen atoms of the ligand and of S201-(5.43).

The 4-ns trajectories of the WT, WT^{U466}, and $R130V^{U466}$ forms from the TXA_2R_{1DISU} set were, finally, subjected to essential dynamics analysis (see the sections below) and employed to produce a number of average structures along each MD trajectory. These average structures were employed for comparative analyses.

Moreover, for both the selected TXA_2R_{1DISU} and TXA_2R_{2DISU} models in their free and agonist-bound forms, the structures averaged over the first 100 ps (i.e., AVG_{f100ps}), last 100 ps (AVG_{l100ps}), and first 1000 ps (i.e., $AVG_{f1000ps}$) were employed as targets of rigid-body simulations with heterotrimeric Gq (see below).

2.3. Rigid-Body Docking Simulations. The analysis of the structural complementarity between the cytosolic domains of the TXA_2R and $Gq_{\alpha\beta1\gamma2}$ was done by exhaustively sampling the rototranslational space of one protein (probe) with respect to the other (target). The receptor was used as a fixed protein (i.e., target), whereas heterotrimeric Gq was allowed to explore all the possible orientations around the cytosolic domains of the target (i.e., probe). The rigid-body docking algorithm ZDOCK was employed.[49,50] The AVG_{f100ps}, AVG_{l100ps}, and $AVG_{f1000ps}$ structures of the WT, WT^{U466}, and the $R130V^{U466}$ forms of both TXA_2R_{1DISU} and TXA_2R_{2DISU} were employed as targets. The Gq_α model employed in this study was a slightly modified version of the one previously obtained by comparative modeling by using the Gi_α structure as a template (PDB code 1GP2[15]).[51] Three alternative backbone conformations of the last six amino acids of the α-subunit were probed, differing in the extension of the α5-helix and in the presence/absence of turns. In detail, the probed conformations included: (a) one with the α5-helix extended till L352, (b) one with the α5-helix extended till Y350, and (c) one with the α5-helix extended till E349 and with Y350 and N351 in a five-turn conformation. The results shown in this study refer to the conformation at point c, because it is consistent with secondary structure predictions by JPRED (http://www.compbio.dundee.ac.uk/~www-jpred/), as far as the length of the α5-helix is concerned, and because it performed better than the others in terms of number of reliable solutions. This selected conformation is similar to that of the homologous C-terminal peptide of Gt_α determined by NMR (i.e., PDB code: 1AQG).[10] Sequence similarity among the C-terminal amino acids of the different α-subunits is such that significant overlaps are expected in the conformations that recognize receptors.[10] The new model of the α-subunit was merged with the βγ-subunits extracted from the $Gi_{\alpha1\beta1\gamma2}$ heterotrimer (i.e., PDB code: 1GP2).[15]

To improve sampling efficiency, the TXA_2R portions 1−50, 64−125, 149−217, and 245−310, corresponding to the transmembrane and extracellular domains, were not taken into account in docking simulations. A rotational sampling interval of 6° was employed, and the best 4000 solutions were retained and ranked according to the ZDOCK score. To filter the most reliable solutions among the 4000 best scored ones, i.e., the Gq orientations fulfilling the membrane topology requirements, a 20 Å distance cutoff between the Cα-atoms of $R130^{TXA2R}$ and $V353^{Gq\alpha}$ was employed.

All the solutions falling below such a distance cutoff were subjected to cluster analysis and visual analysis of the cluster centers (i.e., the solution representative of each clusters), following an approach previously described.[52] A C_α-atom root-mean-square deviation (C_α-RMSD) cutoff of 4.0 Å was employed for clustering. The selected receptor−G protein complexes were energy minimized using the GBSW implicit membrane model.

2.4. MD Simulations of the Heterotrimeric Gq-TXA_2R Complexes. The predicted complexes between Gq and WT^{U466} as well as the receptor-free Gq heterotrimer were subjected to 6 ns MD simulations in implicit membrane/water. The same protocol as the one employed for the isolated receptor was used except for the integration step that was equal to 0.002 ps and the length of the equilibration that was equal to 400 ps.

In addition to the intrahelix distance restraints applied to the receptor, which were the same as those employed for MD simulations on the isolated receptor, intrahelix distance restraints were applied to all the α-helical segments in the $\alpha\beta\gamma$ subunits of Gq.

The starting structure of GDP was extracted from the crystal structure of heterotrimeric Gi_α (PDB code 1GP2[15]) and docked into the homologous nucleotide-binding site of Gq_α. The CHARMM all-atom charge distribution was assigned to the GDP atoms.

Comparative analyses were carried out on the structures averaged over the first 2ns (i.e., AVG_{F2NS}), the second 2ns (i.e., AVG_{S2NS}) and the last 2 ns (i.e., AVG_{L2NS}) of the 6-ns trajectory of the receptor-free and receptor-bound heterotrimeric Gq.

2.5. Essential Dynamics Analysis. The essential motions associated with agonist binding to the TXA_2R and with receptor binding to heterotrimeric Gq were analyzed through the principal component analysis (PCA) of the MD trajectories, implemented in the WORDOM

(43) Takasuka, M.; Kishi, M.; Yamakawa, M. *J. Med. Chem.* **1994**, *37*, 47−56.
(44) Fortier, S. F.; Erman, M. G.; Langs, D. A.; De Titta, G. T. *Acta Crystallogr.* **1980**, *B36*, 1099−1103.
(45) Dewar, M. J. S.; Zoebisch, E. G.; Healey, E. F.; Stewart, J. J. P. *J. Am. Chem. Soc. 3902−3909.* **1985**, *107*, 3902−3909.
(46) Funk, C. D.; Furci, L.; Moran, N.; Fitzgerald, G. A. *Mol. Pharmacol.* **1993**, *44*, 934−9.
(47) Khasawneh, F. T.; Huang, J. S.; Turek, J. W.; Le Breton, G. C. *J. Biol. Chem.* **2006**, *281*, 26951−65.
(48) So, S. P.; Wu, J.; Huang, G.; Huang, A.; Li, D.; Ruan, K. H. *J. Biol. Chem.* **2003**, *278*, 10922−7.
(49) Chen, R.; Li, L.; Weng, Z. *Proteins* **2003**, *52*, 80−7.
(50) Chen, R.; Weng, Z. *Proteins* **2002**, *47*, 281−94.
(51) Fanelli, F.; Menziani, C.; Scheer, A.; Cotecchia, S.; De Benedetti, P. G. *Proteins* **1999**, *37*, 145−56.
(52) Fanelli, F.; Dell'Orco, D. *Biochemistry* **2005**, *44*, 14695−14700.

software.[53] PCA isolates and identifies low frequency, high amplitude movements in the dynamics, separating meaningful concerted motions from noise and high-frequency oscillations. A covariance matrix was constructed by using the Cartesian coordinates of the C_α-atoms as variable set and the trajectory frames as data set. PCA was carried out both on single or concatenated C_α-trajectories, following a procedure already described.[54] As for the receptor protein, all the C_α-atoms were considered both for RMSD minimization and for the building of the covariance matrix (i.e., sequence 1−343). In contrast, for Gq_α, the residue stretches 33−57 and 183−347, corresponding to the Ras-like domain, were considered for the fitting of the C_α-atoms, whereas all the C_α-atoms served to the building of the covariance matrix. This setting concerning Gq_α was instrumental in investigating the effect of receptor binding on the motion of the α-helical domain with respect to the Ras-like domain. The reference structure for both the fitting of the C_α-atoms and calculation of the covariance matrix was the average structure computed over all the frames constituting the concatenated trajectory.

According to the essential dynamics analysis protocol,[54] the diagonalization of the covariance matrix produced a set of eigenvectors and eigenvalue pairs, which indicate, respectively, directions and amplitudes of motions. Eigenvectors characterized by high eigenvalues describe motions with great atomic displacements. The motions along the most significant eigenvectors were obtained by projecting each frame of the original trajectories over the first ten eigenvectors.

3. Results

3.1. Structural Hallmarks of the Inactive and Active State Ensembles of TXA_2R. The first step in this study was predictions of the whole 3D structure of TXA_2R through comparative modeling by using the highest resolution crystal structure of rhodopsin[36] as a template. The very recent release of the crystal structure of the human β2-AR provided us with another potential template for modeling members of the rhodopsin family, including the TXA_2R. However, for TXA_2R, sequence similarity with rhodopsin is significantly higher than that with the β2-AR, making the photoreceptor the proper template. Difficulties in modeling IL1, EL1, EL3, and the N-terminus imposed the building of 1600 models, by probing different short variances of the rhodopsin template associated with the employment of external α-helical restraints. In selected cases, de novo design of EL3 was probed as well. Structural quality checks associated with evaluations of restraint violation led to the selection of 12 receptor models that were used as inputs of MD simulations in implicit membrane/water. Implicit membrane models have recently proved their effectiveness in simulations of integral membrane proteins[55] and are particularly suitable for simulations of GPCRs whose oligomeric order and, consequently, protein/lipid stoichiometry is ill-defined. Good examples of the effectiveness of the approach in terms of structural stability of the simulated proteins have been reported for a number of integral membrane proteins, including bacteriorhodopsin (BRD), which, like GPCRs, is made of seven transmembrane helices. Indeed, the range of backbone RMSDs between starting experimental structure and average structures of monomeric or trimeric BRD simulated in implicit membrane were found to be comparable with those concerning the average structures resulting from explicit membrane simulations.[56,57]

The selected TXA_2R models can be divided into two sets, i.e., one characterized by the presence of one disulfide bridge between C105(3.25) and C183 (in EL2), which was inherited from rhodopsin structure (TXA_2R_{1DISU}) and was consistent with experimental evidence[39] and the other characterized by an additional disulfide bridge between C11 (in the N-terminus) and C102(3.22) (i.e., TXA_2R_{2DISU}). Two models, one from each of the two sets, were employed for the MD setup as well as for docking simulations with the U-46619 agonist (Chart 1) and with heterotrimeric Gq. Given the striking convergence between computations on the two different TXA_2R models, only the results achieved with the model belonging to the TXA_2R_{1DISU} set are shown herein, as they are overall representative of the simulation results.

MD simulations and analyses followed a well-established strategy previously developed to infer the structural hallmarks of functionally different states (i.e., active or inactive) of a number of homologous GPCRs (reviewed in ref 21). The strategy consists in comparative analyses of a large number of average receptor configurations following MD simulations of the empty wild type and of perturbed structures resulting from the introduction of activating or inactivating mutations or from the docking of activating or inactivating ligands. Comparative analyses of such average arrangements are then carried out focusing on a few but significant structural features, which are shared in common by the majority of the receptor forms with similar functionality and which make the difference between inactive and active states (reviewed in ref 21).

Previous applications of this approach converged into the inferences that the interaction pattern of the highly conserved arginine of the E/DRY motif, i.e., R3.50, and the degree of solvent accessibility of selected cytosolic portions are hallmarks of mutation- and ligand-induced inactive and active states of a number of GPCRs of the rhodopsin family. In fact, for the agonist-bound (i.e., active) and the antagonist-bound (i.e., nonactive) forms, the establishment of crucial intermolecular interactions (as suggested by experimental evidence) was found, respectively, concurrent with destabilization and reinforcement of the intramolecular interactions involving the E/DRY arginine in the empty receptor forms (reviewed in ref 21). A destabilization of the R3.50 interactions was also found to be a structural feature of constitutively active mutants (reviewed in ref 21). Ligand- and mutation-induced active states shared also in common an increase in solvent accessibility (compared to the inactive states) of selected amino acids at the cytosolic extensions of H3 and H6 (reviewed in ref 21).[58−61] The role of the Coulombic interactions involving R3.50 in maintaining the inactive states of GPCRs as inferred from our computational experiments is consistent with a number of in vitro and in silico experiments by others.[62−68]

(53) Seeber, M.; Cecchini, M.; Rao, F.; Settanni, G.; Caflisch, A. *Bioinformatics* **2007**.
(54) Amadei, A.; Linssen, A. B.; Berendsen, H. J. *Proteins* **1993**, *17*, 412−25.
(55) Feig, M.; Brooks, C. L., 3rd *Curr. Opin. Struct. Biol.* **2004**, *14*, 217−24.
(56) Tanizaki, S.; Feig, M. *J. Chem. Phys.* **2005**, *122*, 124706.
(57) Tanizaki, S.; Feig, M. *J. Phys. Chem. B* **2006**, *110*, 548−56.
(58) Zhang, M.; Mizrachi, D.; Fanelli, F.; Segaloff, D. L. *J. Biol. Chem.* **2005**, *280*, 26169−26176.
(59) Angelova, K.; Fanelli, F.; Puett, D. *Mol Endocrinol* **2008**, *22*, 126−38.
(60) Zhang, M.; Tao, Y. X.; Ryan, G. L.; Feng, X.; Fanelli, F.; Segaloff, D. L. *J. Biol. Chem.* **2007**, *282*, 25527−39.
(61) Feng, X.; Muller, T.; Mizrachi, D.; Fanelli, F.; Segaloff, D. L. *Endocrinology* **2007**, DOI: 10.1210/en.2007−1341.
(62) Cohen, G. B.; Yang, T.; Robinson, P. R.; Oprian, D. D. *Biochemistry* **1993**, *32*, 6111−5.
(63) Ballesteros, J. A.; Jensen, A. D.; Liapakis, G.; Rasmussen, S. G.; Shi, L.; Gether, U.; Javitch, J. A. *J. Biol. Chem.* **2001**, *276*, 29171−7.
(64) Li, J.; Huang, P.; Chen, C.; de Riel, J. K.; Weinstein, H.; Liu-Chen, L. Y. *Biochemistry* **2001**, *40*, 12039−50.
(65) Visiers, I.; Ebersole, B.; Dracheva, S.; Ballesteros, J.; Sealfon, S. C.; Weinstein, H. *Int. J. Quantum Chem.* **2002**, *88*, 65−75.
(66) Vassart, G.; Pardo, L.; Costagliola, S. *Trends Biochem. Sci.* **2004**, *29*, 119−26.
(67) Flanagan, C. A. *Mol. Pharmacol.* **2005**, *68*, 1−3.
(68) Ramon, E.; Cordomi, A.; Bosch, L.; Zernii, E. Y.; Senin, II;, Manyosa, J.; Philippov, P. P.; Perez, J. J.; Garriga, P. *J. Biol. Chem.* **2007**, *282*, 14272−82.

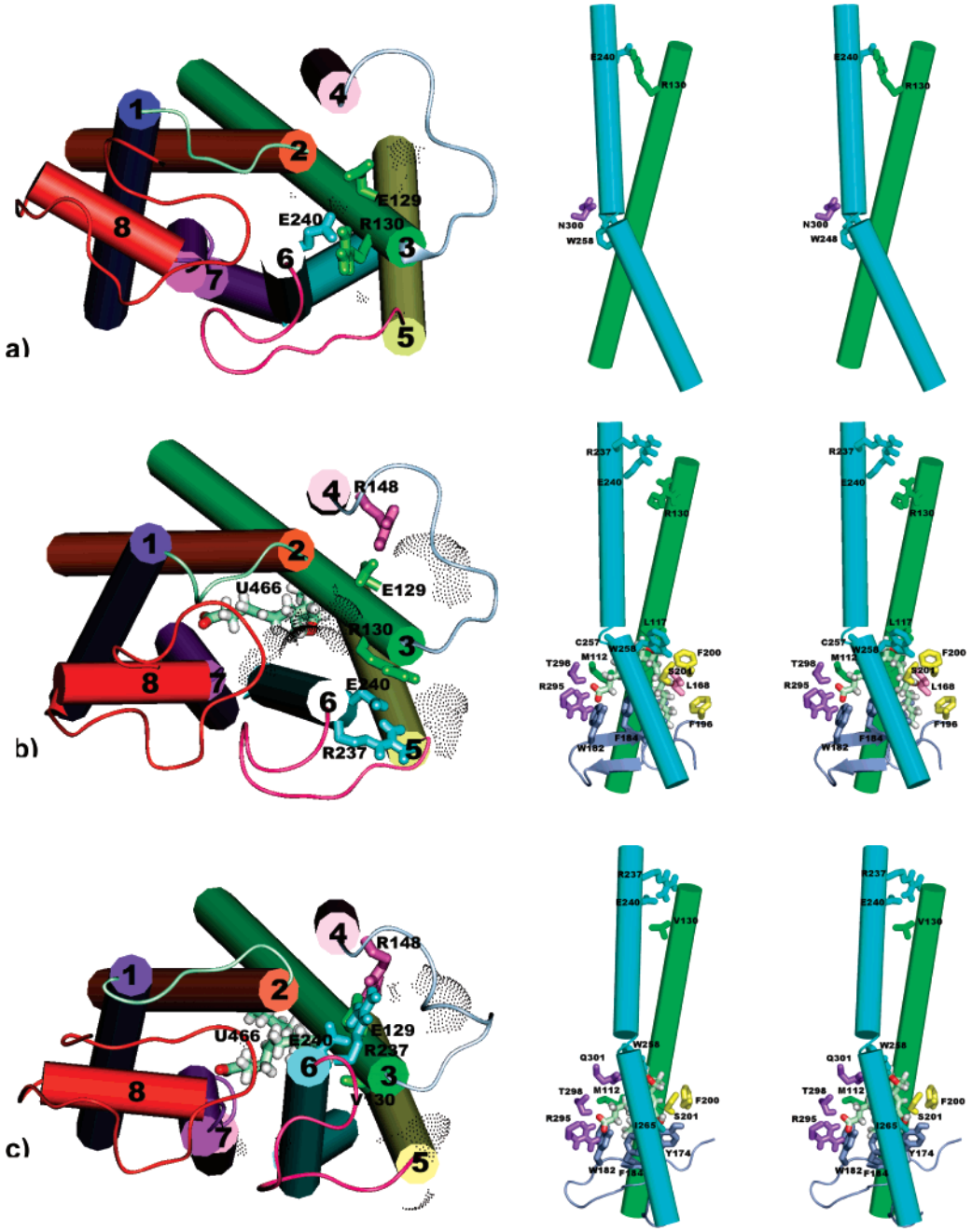

Figure 2. Average minimized structures of WT (a), WT^{U466}, (b) and $R130V^{U466}$ (c). The structures are averaged over the first 500 ps in the second half of a 4-ns trajectory. The choice of this average is because of the high structural similarity (i.e., low C_α-RMSDs) among the frames that participate in the average and because differences in the SAS index among the three receptor forms reach their maximal extent in this phase of the MD trajectory. Left panels: the cytosolic and the seven-transmembrane domains are shown, seen from the intracellular side in a direction perpendicular to the membrane plane. The extracellular domains are not shown. Details of the interaction pattern of E3.49 and R3.50 of the E/DRY motif are shown. The SAS computed over F63-(2.39), I132(3.52), C223(5.65), S239(6.29), and M243(6.33) is represented by gray dots. The SAS values for the WT, WT^{U466}, and $R130V^{U466}$ are 15.0 Å^2, 149.0 Å^2, and 72.0 Å^2, respectively. Right panels: stereoview, in a direction parallel to the membrane plane, of H3 and H6. Drawings highlight the conformational change in W258(6.48) (compared to the empty WT) following the establishment of the interactions between the agonist and selected binding site amino acids of TXA_2R. The U-46619 agonist is represented by sticks and colored by atom-type.

The importance of the anionic and cationic components of the E/DRY motif, i.e., E/D3.49 and R3.50, in receptor function is linked to their high conservation within the members of the rhodopsin family (i.e., 86% and 96% of conservation, respectively).[69] Indeed, the E/DRY glutamate/aspartate resulted to be a switch of GPCR activation through deprotonation/reprotonation equilibria.[70−74] Reprotonation of this conserved amino acid residue is, in fact, suggested to promote the active states in a number of GPCRs.[70−74] On the other hand, the integrity of R3.50 seems to be necessary for receptor signaling (reviewed in refs 34, 66). Whether the main role of the almost fully conserved

(69) Mirzadegan, T.; Benko, G.; Filipek, S.; Palczewski, K. *Biochemistry* **2003**, *42*, 2759−67.
(70) Arnis, S.; Fahmy, K.; Hofmann, K. P.; Sakmar, T. P. *J. Biol. Chem.* **1994**, *269*, 23879−81.
(71) Scheer, A.; Fanelli, F.; Costa, T.; De Benedetti, P. G.; Cotecchia, S. *Proc. Natl. Acad. Sci. U.S.A* **1997**, *94*, 808−13.
(72) Fahmy, K.; Sakmar, T. P.; Siebert, F. *Biochemistry* **2000**, *39*, 10607−12.
(73) Ghanouni, P.; Schambye, H.; Seifert, R.; Lee, T. W.; Rasmussen, S. G.; Gether, U.; Kobilka, B. K. *J. Biol. Chem.* **2000**, *275*, 3121−7.
(74) Knierim, B.; Hofmann, K. P.; Ernst, O. P.; Hubbell, W. L. *Proc. Natl. Acad. Sci. U.S.A* **2007**.

arginine is to maintain the inactive state of the receptor or to allow receptor transition toward the active states or to participate in the receptor−G protein interface is still unclear and may depend on the receptor system (critically analyzed in refs 34, 66).

Because of its well documented importance, the E/DRY motif has been as well the focus of the comparative analyses of the average structural features of WT, WT^{U466}, and $R130V^{U466}$ carried out in this study. Furthermore, for the first time, comparisons of the average structures were done in parallel to the analyses of the essential motions along the concatenated trajectories of the free and agonist-bound forms.

A recurrent feature of the ground state, inherited from the crystal structure of dark rhodopsin, is the double charge-reinforced H-bond between R130(3.50) and both the adjacent E129(3.49) and E240(6.30) (Figure 2). This interaction pattern is associated with an interhelical H-bond between W258(6.48) and N300(7.45), and with the bend at the highly conserved P6.50 (Figure 2). The latter structural feature was inherited from rhodopsin structure as well.

In the WT^{U466} complex, the receptor portions that make contacts with the U-46619 agonist include H3, H4, H5, H6, H7, and EL2. Intermolecular contacts consist essentially in van der Waals attractive interactions. In detail, the most recurrent agonist−receptor interface over the 4-ns trajectory include (a) the interaction between both the α and ω chains of the agonist and F184 (in EL2) and F196(5.38), (b) contacts between the α chain of the agonist and M112(3.32), (c) contacts between the ω chain of the agonist and V171, Y174, L185, (all in EL2), I113(3.33), L168(4.61), F196(5.38), and F200(5.42), (d) contacts between either one of the two chains and L261(6.51), finally, (e) contacts between the cycle of the agonist and L117(3.37), C257(6.47), and W258(6.48) (Figure 2b). The information transfer, however, seems to rely on selected intermolecular H-bonds. In fact, the establishment of the H-bonds between the carboxylate and hydroxy group of the U-46619 agonist and R295(7.40) and S201(5.43), respectively, of the receptor is required to trigger the local perturbations that promote the active state ensembles. The former charge-reinforced H-bond is almost always associated with an additional H-bond between the carboxylate of the agonist and Q177 or W182 (both in EL2) and/or T298(7.43). The most striking local perturbation induced by the agonist is the breakage of the W258(6.48)−N300(7.45) H-bond found in the empty receptor state, following a conformational change of the conserved tryptophan caused by contacts with the agonist (Figures 2b and 3). The conformational change in the W258(6.48) side chain is associated with a change in the bending mode of H6. This effect is marked by a move of C257(6.47) that is oriented toward H7 and the membrane space in the empty WT, whereas it is directed toward the core of the helix bundle in the agonist−receptor complex (Figure 3). Consistent with the advances in structure determination of rhodopsin,[22] these movements at the extracellular half of H6 are not associated with a dramatic separation of the cytosolic extensions of H3 and H6. Perturbations in distal cytosolic domains in response to agonist binding rather include the breakage of both the charge-reinforced H-bonds involving R130(3.50) of the E/DRY motif and an increase in solvent accessibility of selected amino acids at the cytosolic extensions of H3, H5, and H6 (Figures 2 and 4). Indeed, the solvent-accessible surface area (SAS) computed over F63(2.39), I132(3.52), C223(5.65), S239(6.29), and M243(6.33) stays close to 0 $Å^2$ along the 4-ns trajectory of WT, whereas it persists above 100 $Å^2$ along the 4-ns trajectory of WT^{U466} (Figure 4).

Figure 3. Superimposition of WT with WT^{U466} (top), WT with $R130V^{U466}$ (middle), and WT^{U466} with $R130V^{U466}$ (bottom). The structures averaged over the first 500 ps in the second half of a 4-ns trajectory have been employed. Only the seven helices are shown, seen from the intracellular side in a direction perpendicular to the membrane plane. The side chains of C257(6.47) and W258(6.48) are shown. WT, WT^{U466}, and $R130V^{U466}$ are colored in gray, green, and purple, respectively. Drawings were done by means of the software PYMOL 0.97 (http://pymol.sourceforge.net/).

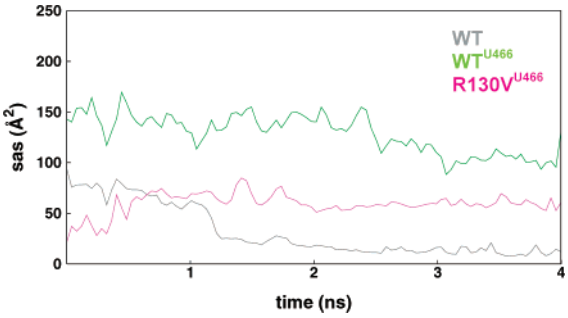

Figure 4. Plot of the SAS index vs the simulation time. The SAS index computed over F63(2.39), I132(3.52), C223(5.65), S239(6.29), and M243(6.33) along the 4-ns trajectories of WT (gray line), WT^{U466} (green line), and $R130V^{U466}$ (magenta line) are shown.

Monitoring the dihedral angles in the α and ω chains of the agonist along the trajectory reveals limited rotational variability around the single bonds adjacent to the two double bonds (i.e.,

the τ3, τ5, τ7, and τ9 torsion angles, Supporting Information: Figure 1). Also τ1 stays persistently in the trans (t) conformation, being immobilized by the charge-reinforced H-bond between the carboxylate of the ligand (involved in τ1) and R295(7.40) of the receptor. The flexibility of the U-46619 agonist essentially resides in the last three torsion angles of the ω chain (i.e., τ11, τ12 and τ13), which tend to move from the t to gauche$^+$ (g^+) or gauche$^-$ (g^-) conformations (Supporting Information: Figure 1), thus allowing the terminal part of the chain to explore different areas of the receptor binding site.

Interestingly, the R130V^{U466} form is characterized by a different orientation of the extracellular half of H6, compared to WT^{U466} (Figures 2 and 3). This difference is marked by the different positions and conformation of C257(6.47) and W258(6.48) that, in the R130V^{U466} structure, are more similar to WT than to WT^{U466} (Figures 2 and 3). Moreover, R130V^{U466} is characterized by the absence or a reduction of contacts between the agonist and H4 and H5, respectively, compared to WT^{U466} (Figure 2). Looking at the cytosolic domains, R130V^{U466} is characterized by a SAS index persistently higher than that of WT but lower than that of WT^{U466} (Figures 2 and 4).

Collectively, the results of computation are indicative of a structural connection between the agonist binding site and the cytosolic interface between H3 and H6, which holds the E/DRY motif. The intramolecular communication between these distal sites is two-way in the sense that the establishment of a few privileged interactions between the agonist and the receptor is associated with changes in the interaction pattern and solvent accessibility of selected amino acids in the cytosolic domains, whereas, vice versa, a perturbation in the cytosolic domains, such as valine substitution for R130(3.50), is associated with a change in the reciprocal orientation of the extracellular halves of H3, H4, H5, and H6 that participate in the agonist binding site (Figures 2 and 3).

Agonist docking into either the WT or the R130V mutant results in an augmentation of the average C_α-RMSD from the energy-minimized input receptor structure (Supporting Information: Figure 2). In fact, the C_α-RMSD computed over the whole structure (i.e., black lines in Supporting Information: Figure 2) stays around 3 Å in the 4-ns trajectory of WT, whereas it stays around 4 Å in both the trajectories of WT^{U466} and R130V^{U466} (Supporting Information: Figure 2). For all three receptor forms, a decrease of about 1 Å is observed if C_α-RMSDs are computed over the transmembrane domains (gray lines in Supporting Information: Figure 2). Collectively, these results are indicative of higher deviations from the input structure in the agonist-bound states compared to the empty receptor state.

3.2. Selected Structural Hallmarks of the Inactive and Active Receptor States Correlate with the Complementarity for the G Protein. The intrinsic structural differences between the three different TXA_2R forms were interpreted in the context of interaction models with the cognate G protein (Gq) following rigid-body docking simulations. In this respect, the AVG_{f100ps}, AVG_{l100ps}, and $AVG_{f1000ps}$ structures of the selected TXA_2R_{1DISU} and TXA_2R_{2DISU} models in their free and agonist-bound forms were employed as targets of rigid-body docking simulations with heterotrimeric Gq. Docking simulations and analyses followed an approach recently developed for predicting likely contacts between the crystal structure of dark rhodopsin and heterotrimeric Gt.[52,75] Only the results achieved with the $AVG_{f1000ps}$ structure of the TXA_2R_{1DISU} in its WT, WT^{U466}, and R130V^{U466} forms are shown herein since they overlap significantly with the results achieved by employing the alternative average structures and are also significantly representative of the results achieved with the free and agonist-bound forms of the TXA_2R_{2DISU} models.

For all three receptor forms, a distance-based filter discharged more than 96% of the 4000 best scored solutions. Cluster analysis, followed by visual inspection of the cluster centers, resulted in a further elimination of false positives (i.e., the docking solutions acceptable according to the docking score but not realistic). Indeed, for each run, only one cluster was found to contain realistic solutions, i.e., consistent with the expected membrane topology of Gq. Acceptable membrane topologies were considered those characterized by the main axis of the N-terminal α-helix of Gq$_\alpha$ (i.e., the αN-helix (Figure 1a)) almost parallel and close enough to the membrane surface to allow the post-translational hydrophobic modifications of the α- and γ-subunits to insert into the membrane. The highest scored solution from this cluster, concerning the WT, WT^{U466}, and R130V^{U466} forms, are shown in Figure 5.

The results of rigid-body docking simulations reflect the main inferences from MD analyses on the isolated receptors. Indeed, consistent with the increase in the SAS index shown by the WT^{U466} form compared to the empty WT form, the C-terminus of Gq$_\alpha$ penetrates the interface between H3 and H6 only in the complex involving WT^{U466}, where it establishes contacts with the arginine of the E/DRY motif (Figures 5 and 6). In contrast, in the complexes, which involve the WT and R130V^{U466} forms, the C-terminus of Gq$_\alpha$ docks, respectively, on IL1 and the cytosolic end of H4. Furthermore, in the best complex involving R130V^{U466}, the membrane topology of the G protein is not much reliable, since the N-terminus of Gq$_\alpha$ and the C-terminus of Gq$_\gamma$ are not sufficiently close to the putative membrane surface. Considering that this complex is the best representative of the most reliable complexes involving R130V^{U466}, it can be inferred that the R130V mutant has lower complementarity for Gq$_\alpha$ than the WT. The extent of contacts between Gq$_\alpha$ and the receptor displays the same trend as that of the SAS index, i.e., WT^{U466} > R130V^{U466} > WT (Figures 2, 4, and 5). In this respect, in the WT^{U466}−Gq$_\alpha$ complex, the following receptor and Gq$_\alpha$ portions participate in the receptor−G protein interface: (a) IL1 of WT^{U466} makes contacts with the end of the αN-helix/beginning of the β1-strand of Gq$_\alpha$; (b) the cytosolic extensions of H3 and H6 of WT^{U466} make contacts with the C-terminus of the α5-helix of Gq$_\alpha$; (c) H6 of WT^{U466} makes contacts with the α4/β6 loop of Gq$_\alpha$; (d) the C-tail of WT^{U466} makes contacts with the α2/β4 and α3/β5 loops of Gq$_\alpha$ (Figures 5 and 6).

The architecture of the WT^{U466}−G protein complex predicted in this study, as far as the docking mode of the α5-helix and the membrane topology of the αN-helix is concerned, is mostly consistent with predictions on the rhodopsin−transducin system made by us[52,75] and others.[76−78]

Collectively, the results of this study suggest that, in the agonist-bound states of WT TXA_2R, the release of the intramo-

(75) Dell'Orco, D.; Seeber, M.; Fanelli, F. *FEBS Lett.* **2007**, *581*, 944−8.
(76) Filipek, S.; Krzysko, K. A.; Fotiadis, D.; Liang, Y.; Saperstein, D. A.; Engel, A.; Palczewski, K. *Photochem. Photobiol. Sci.* **2004**, *3*, 628−38.
(77) Nikiforovich, G. V.; Taylor, C. M.; Marshall, G. R. *Biochemistry* **2007**, *46*, 4734−44.
(78) Slusarz, R.; Ciarkowski, J. *Acta Biochim. Pol.* **2004**, *51*, 129−36.

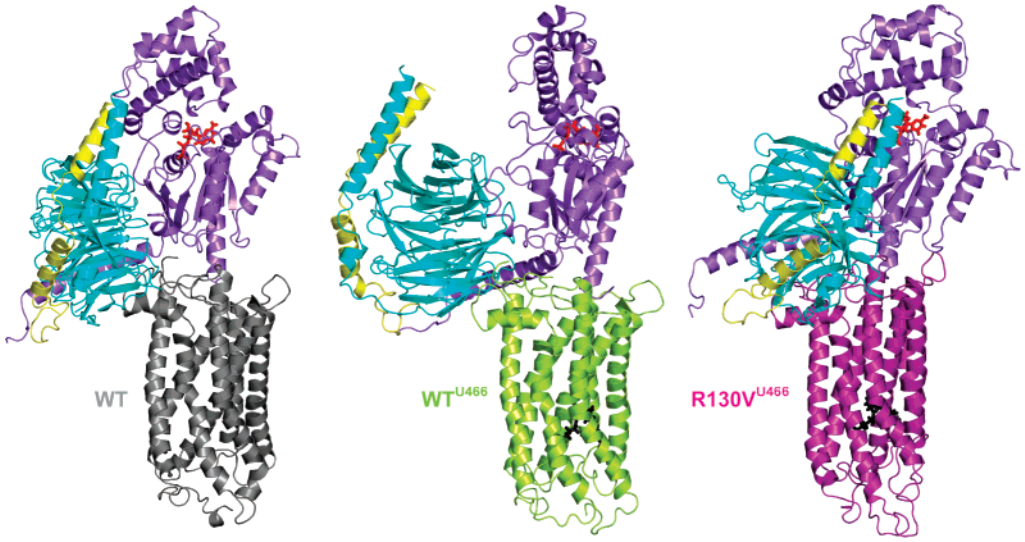

Figure 5. Best predicted receptor−G protein complexes by rigid-body docking. Side view in a direction parallel to the membrane surface of the best predicted complex between heterotrimeric Gq and the three different TXA_2R forms, i.e., WT (left panel, colored in gray), WT^{U466} (middle panel, colored in green), and R130V^{U466} (right panel, colored in purple). The α-, *β*-, and *γ*-subunits of Gq are colored in violet, cyan, and yellow, respectively. The GDP nucleotide is colored in red, whereas the U-46619 agonist is colored in black. Drawings were done by means of the software PYMOL 0.97 (http://pymol.sourceforge.net/).

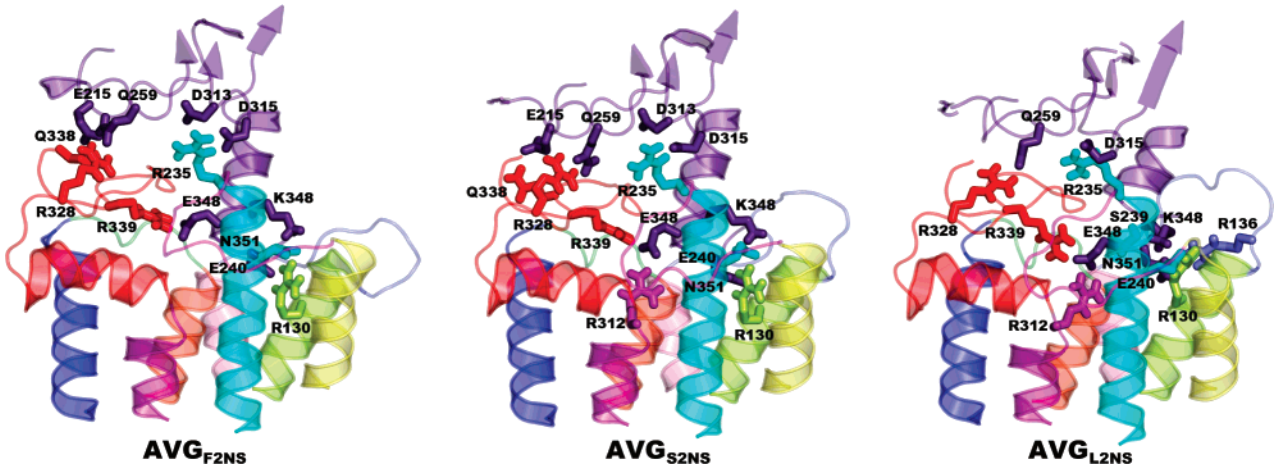

Figure 6. Predicted average minimized structures of the complexes between Gq and WT^{U466}. Side view, in a direction parallel to the membrane surface, of the Gq-WT^{U466} interface in the AVG$_{F2NS}$, AVG$_{S2NS}$, and AVG$_{L2NS}$ structures. As for heterotrimeric Gq, only the interface amino acids of the α-subunit are shown in violet. These amino acids belong to the α2/*β*4, α3/*β*5, α4/*β*6 and the C-terminus of the α5-helix. Selected details of the interactions are shown. As for the receptor, only the cytosolic half is shown. H1, H2, H3, H4, H5, H6, H7, and H8 are, respectively, colored in blue, orange, green, pink, yellow, cyan, purple, and red. The C-tail is colored in red as well, whereas IL1, IL2, and IL3 are colored in lime, slate, and magenta, respectively. Drawings were done by means of the software PYMOL 0.97 (http://pymol.sourceforge.net/).

lecular interactions by the arginine of the E/DRY motif and the associated increase in solvent exposure of the cytosolic ends of H3, H5, and H6 favor the approach of the C-tail of Gq$_\alpha$ to the conserved arginine. These results, together with the observation that the replacement of the conserved arginine results in a less marked opening of the cytosolic crevice and in a poorly reliable receptor−G protein complex, are indicative of a double role of R130(3.50), i.e., switch of receptor activation (essential player in the intramolecular communication), and an essential recognition point for the G protein (mediator of the intermolecular communication).

3.3. Intermolecular Communication between the Receptor and the G Protein. To infer the effects of receptor interaction on the dynamics of Gq$_\alpha$, 6-ns MD simulations in implicit membrane/water were carried out on of the WT^{U466}-bound form of heterotrimeric Gq (i.e., the best predicted WT^{U466}−G protein complex) and on the receptor-free heterotrimer. Trajectory analysis focused on the α-subunit. Similar to the isolated receptor forms, comparisons of the two trajectories involving Gq relied on the analyses of a number of average structures, and on PCA analyses of the trajectory resulting from the concatenation of the trajectories of the free and receptor-bound Gq.

The C$_\alpha$-RMSD of the whole Gq$_\alpha$ stays on average between 3 Å and 4 Å in the receptor-free form, whereas it stays between 4 Å and 5 Å in the receptor-bound form (results not shown).

A first inference on the structure and dynamics of Gq$_\alpha$ in response to receptor binding is derived from a DynDom[79,80] comparative analysis of the AVG$_{F2NS}$ and AVG$_{L2NS}$ of both the free and the receptor-bound forms of Gq (Figure 7). This analysis found a rotation of the α-helical domain with respect to the Ras-like domain as a remarkable difference between receptor-bound and receptor-free forms. The rotation axis was

(79) Hayward, S.; Berendsen, H. J. *Proteins* **1998**, *30*, 144−54.
(80) Hayward, S.; Kitao, A.; Berendsen, H. J. *Proteins* **1997**, *27*, 425−37.

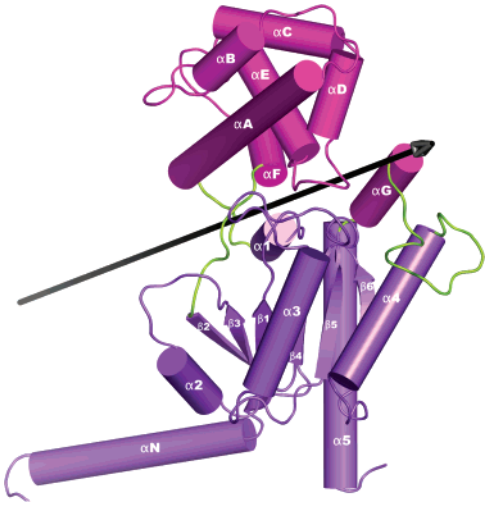

Figure 7. Domain motions in Gq_α. Interdomain rotation axis resulting from the DynDom analysis carried out on the AVG_{F2NS} and AVG_{L2NS} of receptor-bound G protein. The axis has been drawn on the AVG_{F2NS} structure. Violet, magenta, and green indicate, respectively, RAS-like domain, α-helical domain, and linkers. Noel's nomenclature[12] is also shown. Drawings were done by means of the software PYMOL 0.97 (http://pymol.sourceforge.net/).

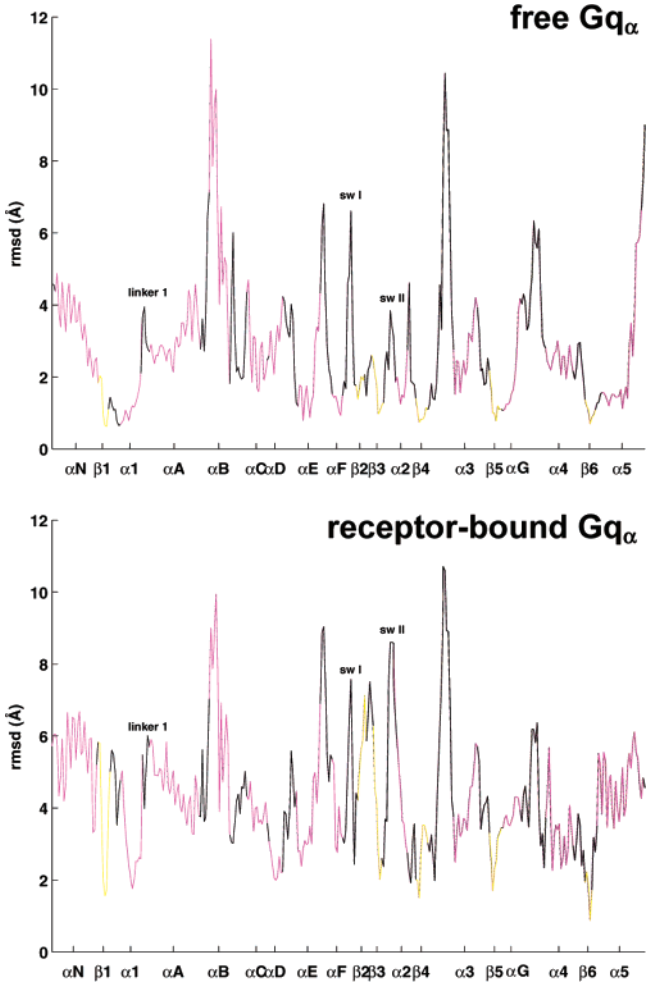

Figure 8. Average C_α-RMSD versus amino acid residues. Plots of the C_α-RMSD averaged over the C_α-RMSD of all the frames in the 6-ns trajectories of the receptor-free (top) and receptor-bound (bottom) forms of Gq_α. The whole receptor sequence has been considered for the C_α-atom fitting between each frame and the minimized coordinates of the input structure. Lines are colored according to the secondary structure elements, where magenta, yellow, and black indicate α-helices, *β*-strands, and loop regions. Ticks on the *x*-axis indicate the central residue in the secondary structure elements, which are labeled according to Noel's nomenclature.

located between the two domains, almost parallel to the main axis of the αA-helix. The bending regions included switch I (Figure 7).

A significant contribution to the comparisons of the G protein dynamics in the absence and presence of the receptor comes from the plots of the average C_α-RMSD per Gq_α residue (Figure 8). These deviations were computed with respect to the minimized coordinates (i.e., prior to MD simulations) of Gq_α, by considering the entire Gq_α sequence. Comparisons of the RMSD profiles of the free and receptor-bound forms of Gq_α highlight receptor-induced motions of the following Gq_α portions: αN-helix, *β*1-strand, *β*1/α1 loop, α1-helix, α1/αA loop (i.e., linker1), αA-helix, αE-helix, αE/αF loop, αF-helix, αF/*β*2 loop (i.e., linker 2 or switch I), *β*2-*β*3 hairpin, *β*3/α2 loop (i.e., switch II), α2-helix, αG-helix, *β*6/α5 loop, and α5-helix (Figure 8). The α5-helix undergoes remarkable deviations from the input structure both in the free and receptor-bound forms (Figure 8). The causes and extents of these deviations are, however, different in the free and receptor-bound Gq. In fact, in the receptor-free form, such deviations concern the last 10 amino acids and are due to the progressive establishment of intramolecular interactions between the C-tail of Gq_α and (a) the αN-helix (i.e., the interaction between R28 and the backbone carboxylate of V353), (b) the N-terminus of the *β*1-strand (i.e., the K35−E349 salt bridge), and (c) the α4/*β*6 loop (i.e., the D315−K348 interaction). In contrast, in the receptor-bound form, deviations concern the whole helix and are due to the establishment of intermolecular interactions with the receptor.

Consistent with the RMSD profiles, the superimposition of the average structures of the free and receptor-bound forms of Gq_α highlights the receptor-induced deviations of αN-helix, *β*1-strand, *β*1/α1-loop, α1-helix, linker 1, switches I and II, *β*2-*β*3-hairpin, α2-helix, αG-helix, *β*6/α5 loop, and α5-helix, as well as the motion of the α-helical domain relative to the Ras-like domain (Figure 9).

The receptor-induced motions of the Gq domains depend on the establishment of contacts between multiple receptor and Gq_α portions. Selected receptor−G protein interactions established along the MD trajectory suggest potential allosteric pathways within Gq_α. In this respect, the effects on the *β*1-strand motion, associated with the motion of the *β*1/α1 loop, α1-helix, and linker 1, may be consequences, at least in part, of limited contacts between cytosolic amino acids of the receptor and the junction between αN-helix and *β*1-strand. These include (a) the H-bond between $R60^{TXA2}$ and $R28^{Gq\alpha}$ or $K27^{Gq\alpha}$, and (b) the H-bond between $T337^{TXA2}$ and the backbone oxygen atom of $R28^{Gq\alpha}$. This interaction is persistent over the first 2-ns and is successively replaced by the interaction between $T337^{TXA2}$ and $E33^{Gq\alpha}$ (at the N-terminus of the *β*1-strand). The involvement of $R60^{TXA2}$ in G protein recognition is consistent with evidence from in vitro experiments.[81] The effects on the αG-helix motion may arise from interactions between the receptor C-tail and the α3/*β*5 loop. Representatives, in this respect, are the $Q343^{TXA2}$−$Q259^{Gq\alpha}$ and $Q343^{TXA2}$−$R328^{Gq\alpha}$ interactions that characterize, respectively, the first and second nanoseconds (Figure 6). The

(81) Hirata, T.; Kakizuka, A.; Ushikubi, F.; Fuse, I.; Okuma, M.; Narumiya, S. *J. Clin. Invest.* **1994**, *94*, 1662−7.

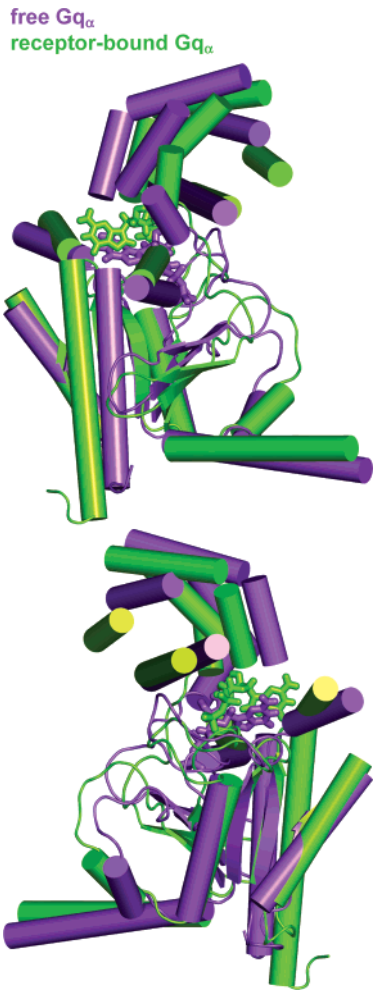

Figure 9. Superimposed averaged structures. Two views of the superimposed AVG_{S2NS} of the free (violet) and receptor-bound forms of Gq_α are shown. To save clarity, the interconnecting loops in the α-helical domain and the αG/α4 loop are not shown. Drawings were done by means of the software PYMOL 0.97 (http:// pymol.sourceforge.net/).

effects on the motion of the α2-helix and switch II are likely due, at least in part, to the interactions between two amino acids in the C-tail of TXA_2R, i.e., $Q343^{TXA2R}$ (in the first 2 ns) or $Q338^{TXA2R}$ (in the remaining part of the 6-ns trajectory) and $E215^{Gq\alpha}$ (in the α2/β4 loop, Figure 6). Finally, the effects on the motion of the β6/α5 loop, which is marked by the establishment of the K270−D327 salt bridge not found in the receptor-free form, are likely due to the interactions between the cytosolic extensions of H3 and H6 of the receptor and the α4/β6 loop as well as the C-terminus of the α5-helix. These include the interactions between $R235^{TXA2}$ and both $D313^{Gq\alpha}$ and $D315^{Gq\alpha}$ (in the α4/β6 loop), as well as the $R130^{TXA2}$−$N351^{Gq\alpha}$ and $E240^{TXA2}$−$K348^{Gq\alpha}$ interactions involving the C-terminus of Gq_α.

Interestingly, the receptor-induced motions of the α5-helix also affect the motion of the β2-β3 hairpin and, consequently, the motion of switches I and II, which are, respectively, connected with the N-terminus of the β2-strand and the C-terminus of the β3-strand (Figures 7−10). In fact, the β2-β3 hairpin is connected with the α5-helix by short-range interactions that change on going from the free to the receptor-bound form of Gq_α. In detail, the interactions between F335 (in the α5-helix) and F195 (in the β2-strand), and between L343 (in the α5-helix) and V193 (in the β3-strand), present in the input structure and in the trajectory of the receptor-free Gq_α are replaced by H-bonds between S192 (in the β2-β3 turn) and both K339 and D340 (in the α5-helix) (Figure 10). We hypothesize that, upon interacting with the receptor, the α5-helix pulls the β2-β3 hairpin at the β2-β3 turn. Such a move of the β2-β3 hairpin results in a conformational change of switch I that pushes up the αF-helix, and in a movement of switch II that is pushed toward the G_α−G_β interface (Figure 10). Furthermore, the motion of the β2-β3 hairpin results in a separation of both the N-terminus of the β2-strand/C-terminus of switch I and the C-terminus of the β3-strand/N-terminus of switch II from the β1/α1 loop. This has been inferred by monitoring the C_α-distances between G42 (in the β1/α1 loop) and both I183 (in the β2-strand) and D199 (in the β3-strand). In fact, the G42−I183 and G42−D199 C_α-distances stay on average around 12 Å and 11 Å, respectively, in the 6-ns trajectory of the receptor-free form, whereas they increase around 19.0 Å and 16 Å, respectively, in the 6-ns trajectory of the receptor-bound form (Figure 10).

Collectively, the effects of the receptor on the motions of linker1, switch I, and switch II are mediated by contacts with multiple portions of the Ras-like domain, i.e., the C-terminus of the αN-helix/N-terminus of the β1-strand, the α2/β4, α3/β5, and α4/β6 loops as well as the C-terminus of the α5-helix. Most relevant in this respect and consistent with experimental evidence[32,33] seems to be receptor interaction with the α5-helix that affects directly the motion of the β6/α5 loop and indirectly, i.e., via the interaction with the β2-β3 hairpin, the motion of both switches I and II.

The clear differences between the average arrangements of the free and receptor-bound forms are accounted for by the first and second eigenvectors arising from the PCA of the concatenated trajectories of the receptor-free (i.e., first 6000 frames) and receptor-bound (i.e., last 6000 frames) forms of Gq_α (Figure 11). Indeed, the first eigenvector is characterized by a clear separation between the two ensembles of configurations from the two concatenated trajectories. The separation between the two sets of displacements is essentially due to persistent structural differences between free and receptor-bound Gq_α ensembles. The displacement distributions concerning the trajectories of the receptor-bound forms (i.e., frames 6000−12000) along the first and second eigenvectors are indicative of essential motions (Figures 11 and 12). These motions include a rotation of the α-helical domain with respect to the Ras-like domain (Figure 11). The rotation axis is, indeed, located between the two domains, almost parallel to the main axis of the αA-helix, consistent with the results of DynDom analysis (Figures 7 and 12). This interdomain rotation, which also characterizes the receptor-free form though by a lesser extent compared to the receptor-bound states, seems to be an intrinsic feature of the Gq_α subunit independent of its communication with the receptor. The latter seems to be instrumental in increasing such motion.

Overall, receptor-induced motions of the β1/α1 loop and of the α1- and αF-helices seem to push the GDP toward the cytosol and increase its solvent accessibility. The nucleotide is, indeed, anchored to (a) the β1/α1 loop by an H-bond between the backbone hydrogen-atom of E43 and one of the three β-phosphate oxygen atoms, (b) the α1-helix by interactions between the β-phosphate oxygen atoms and both K46 and S47, and (c) the αF-helix by interactions between the hydroxy O2′ (in the first 2 ns) or O4′ (in the last 4 ns) oxygen atoms and R175 (Figure 13). The push of the GDP toward the cytosol is

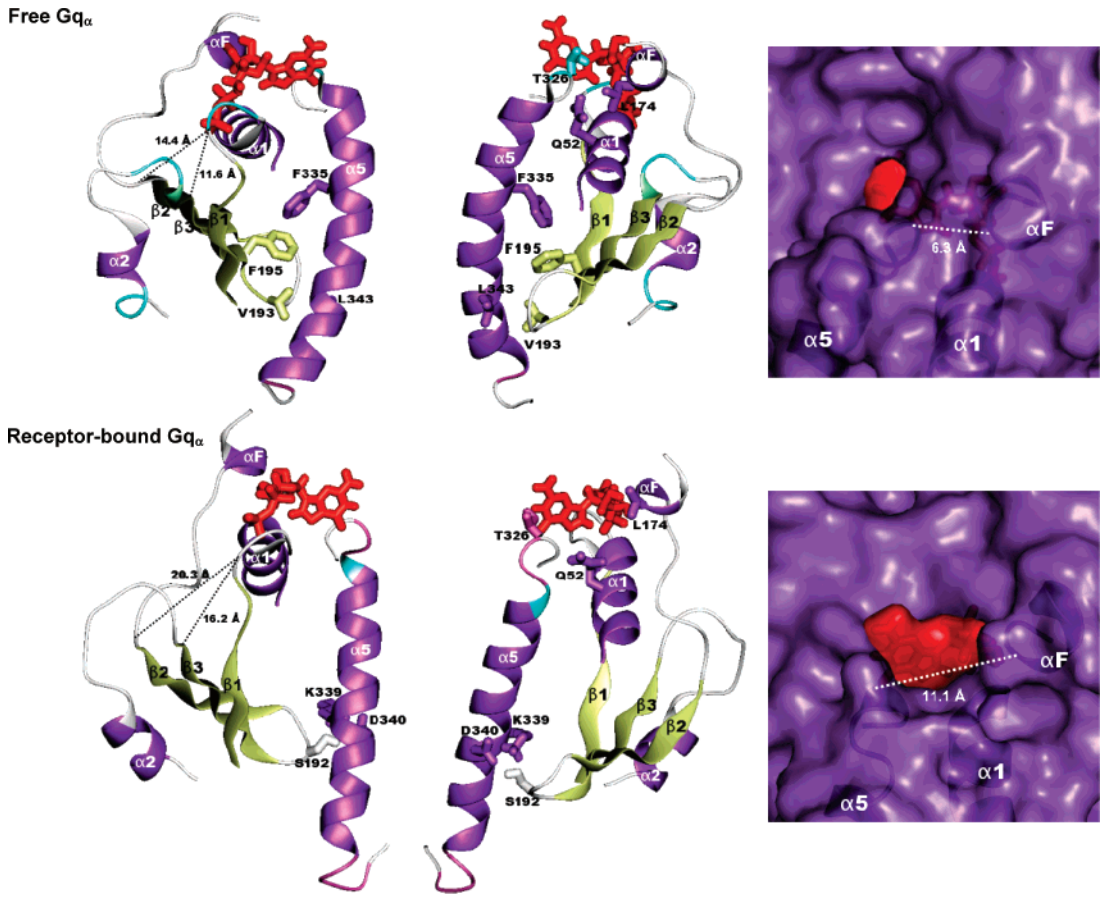

Figure 10. Effects of receptor binding on the dynamics of Gq_α. Details of Gq_α from the AVG_{S2NS} structures concerning the receptor-free (top) and receptor-bound forms (bottom). Only the β1-strand, the β1/α1 loop, the α1-helix, the αF-helix, switch I, the β2-β3 hairpin, switch II, the α2-helix, the β6/α5 loop, and the α5-helix are shown in the left and middle panels. The G protein domains are colored according to secondary structure, i.e., violet, yellow, pink and cyan indicate, respectively, α-helices, β-strands, 4-turns and 3-turns. GDP is colored in red. These domains have been selected as they undergo motions that correlate with the formation of a GDP exit route in response to receptor binding. Selected side chains that make different interactions between the β2-β3 hairpin and the α5-helix on going from the free to the receptor-bound forms are shown both in the left and middle panel. The distances between G42 (in the β1/α1 loop) and both I183 (in the β2-strand) and D199 (in the β3-strand) are shown as dashed lines in the left panels on the structures of both the free (i.e., 14.4 Å and 11.6 Å, respectively, top) and receptor-bound (i.e., 20.3 Å and 16.2 Å, respectively, bottom) forms. In the middle panel, the side chains of Q52 (in the α1-helix), L174 (in the αF-helix), and T326 in the β6/α5 loop are shown, as they undergo significant solvent exposure on going from the free to the receptor-bound form. The SAS computed over them in the AVG_{S2NS} structure is, indeed, 20.0 $Å^2$ in the receptor-free form (top), whereas it becomes 222.0 $Å^2$ in the receptor-bound form (bottom). The right panel shows the contact surface of Gq_α (colored in violet) and that of GDP in red. A zoom has been done on the predicted GDP exit route. Cartoons of α1-, αF-, and α5-helices as well as of the β5/α5 loop are also shown. Dashed white line indicates the C_α-distance between L174 (in the αF-helix) and T326 (in the β6/α5 loop). Such distance stays on average around 6.3 Å in the trajectory of the receptor-free form (top), whereas it stays around 11.1 Å in the trajectory of the receptor-bound form (bottom).

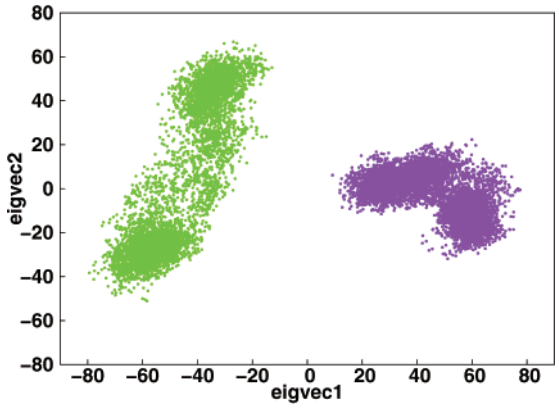

Figure 11. Plots of the displacements along the first and second eigenvectors, arising from PCA. Motions along the two eigenvectors arise from the concatenated C_α-atom trajectories of the free (violet dots) and receptor-bound forms (i.e., green dots).

associated with a receptor-induced straightening of the β1-strand and β1/α1 loop (Figure 10). Markers of the receptor-induced motion of the β1/α1 loop and of the α1-, αF-, and αG-helices, which all participate in the nucleotide binding site, are the replacements of the salt bridges found in the trajectory of the receptor-free form between E43 (in the β1/α1 loop) and R177 (in switch I), as well as between D149 (at the N-terminus of αE-helix) and K269 (in the β5/αG loop), respectively, with the E43−K269 (in the β5/αG loop) and the D149−R175 (in αF-helix) interactions (Figure 13). The access of GDP to the cytosol is favored by the formation of a putative exit route in between the αF-helix and the β6/α5-loop. In fact, conformational changes in the α1/β1 loop and in switch I push up, respectively, the α1- and αF-helices. The former interposes between the αF-helix and the β6/α5 loop, giving solvent accessibility to the anchored nucleotide (Figure 10). Markers of the significant detachment between αF-helix and β6/α5 loop, on going from the free to the bound-receptor forms of Gq_α, are the C_α-distance between L174 (in the αF-helix) and T326 (in the β6/α5 loop) and the correlated solvent accessibility of Q52 (in the α1-helix), L174 (in the αF-helix), and T326 (in the β6/α5 loop). The

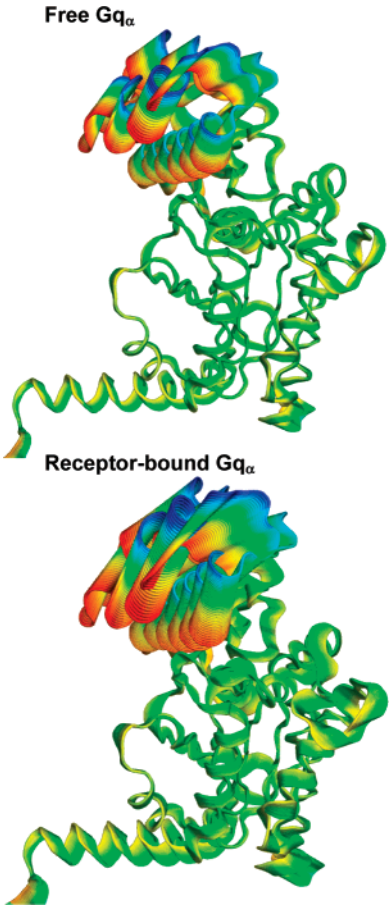

Figure 12. C_α-displacements of Gq in its free (top) and receptor-bound (bottom) states along the second eigenvector from a PCA run on a concatenated trajectory made of 12000 frames. A number of conformations were generated between the minimum and maximum projection on the selected eigenvector. The conformations were then displayed simultaneously, colored according to the factor $\beta_{in} = \gamma_i n + \alpha_i$, where i and n refer to the residue and conformation number, respectively, γ_i is the contribution of residue i to the loadings vector that defines the eigenvector and α_i is a correction factor to center the range of values around 0. The width and color range of the ribbon resulting from the displayed conformations are, thus, proportional to the contribution of the residue to the eigenvector. The direction of the motion described by the eigenvector itself is from red to blue. Drawings were done by means of the software PYMOL 0.97 (http://pymol.sourceforge.net/).

former stays on average around 6.3 Å in the trajectory of the receptor-free form, whereas it stays around 10.6 Å in the trajectory of the receptor-bound form (Figure 10). Consistently, Q52, L174, and T326 stay buried in the receptor-free form (i.e., average SAS computed over them = 16.0 Å^2), whereas they undergo solvent exposure in the receptor-bound form (i.e., average SAS = 205 Å^2), marking the opening of a solvent exposed crevice in the nucleotide binding site (Figure 10). Such formation of a putative nucleotide exit route seems to be linked also to the receptor-induced increase in the mobility of the α-helical domain with respect to the Ras-like domain. Predictions on the GDP exit site were also based on the observed increase in solvent accessibility of GDP in the receptor-bound ensembles of Gq_α compared to the receptor-free ones (Supporting Information: Figure 3).

The distal effects of the receptor on the GDP binding site are, in turn, associated with distal effects of Gq_α on the conformational preferences and interaction pattern of the receptor agonist (Supporting Information: Figure 4). The latter

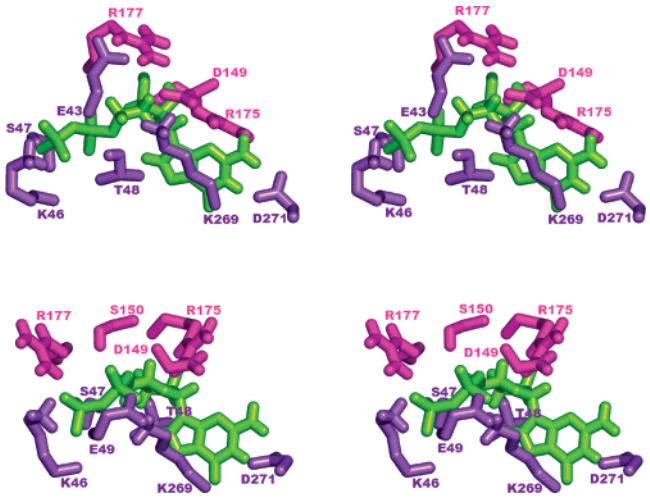

Figure 13. Stereoviews of details of the GDP interactions are shown, which have been extracted from the AVG_{S2NS} of the free (top) and receptor-bound (bottom) forms. The GDP molecule is in green whereas amino acids from the Ras-like and α-helical domains are in violet and magenta, respectively. Drawings were done by means of the software PYMOL 0.97 (http://pymol.sourceforge.net/).

undergoes a conformational transition at the $\tau 3$ and $\tau 5$ torsion angles in the α chain (i.e., from 120.86 ± 9.00 and 120.81 ± 7.92° to −119.09 ± 8.44 and −127.63 ± 7.65°, respectively) after the third nanosecond (Supporting Information: Figure 4). Collectively, in the WT^{U466}−Gq_α complex, the $\tau 2$ and $\tau 10$−$\tau 13$ dihedrals display higher flexibility compared to the WT^{U466} isolated form (Supporting Information: Figures 1 and 4).

4. Discussion

This study represents the first attempt to couple, by computational modeling, the mechanisms of intramolecular and intermolecular communication concerning the GEF TXA_2R and the cognate G protein (Gq) in its heterotrimeric GDP-bound state. The resolution level of the inferences from this study is expected to be higher than that of recent elegant SDSL experiments aimed at mapping the allosteric connection from the receptor to the nucleotide binding pocket of Gi_α.[32,33] Indeed, our study relies on a well-established computational approach consisting of comparative modeling and ligand−protein and protein−protein docking followed by MD simulations in implicit membrane/water and extensive MD analyses. Comparative modeling was instrumental in achieving reliable input structures of the isolated receptors and of the Gq_α, whereas docking simulations were instrumental in predicting likely ligand−receptor and receptor−G protein complexes. MD simulations and analyses on the free and complexed forms of the receptor were aimed at inferring hypotheses on the structural differences between inactive and ligand-induced active receptor states as well as on the effects of receptor binding on the structure and dynamics of Gq_α. In this respect, the employment of implicit membrane models and the application of intrahelix distance restraints both on the receptor and the G protein (see Methods) were instrumental in reducing the system's degrees of freedom and facilitating the detection of essential motions or structural changes correlated with receptor and G protein functionality.

An outcome of MD simulations of the free and agonist-bound forms of the isolated receptor is that the establishment of a few peculiar interactions in the agonist binding site in the extracel-

lular half of the receptor is associated with structural perturbations in the cytosolic extensions of H3, H5, and H6, in the neighborhoods of the highly conserved E/DRY motif. The major perturbations associated with the WT^{U466} form include the weakening of the salt bridge interaction found in the empty WT between R130(3.50) and E240(6.30). The role of the charge-reinforced H-bond between R3.50 and E6.30 in maintaining the inactive states of GPCRs has been overemphasized by a number of computational and in vitro experiments (reviewed in ref 21), including a recent in vitro mutational analysis on rhodopsin.[68] An important structural hallmark of the ligand-induced active states of TXA_2R is the increase in solvent accessibility, compared to the empty (inactive) states, of the cytosolic extensions of H3, H5, and H6. This effect is accounted for by the SAS index, which stays close to 0 $Å^2$ in the free receptor state, increasing above 100 $Å^2$ in the agonist-bond forms (Figures 2 and 4). This result is consistent with computational experiments on mutation-induced activation of the lutropin receptor (LHR)[58−61,82,83] and ligand-induced activation of the melanine-concentrating hormone receptor (MCHR),[84] as well as with very recent advances in structure determination of rhodopsin.[22]

The intramolecular communication between agonist-binding site and cytosolic domains appears to be mediated by the highly conserved P6.50, which introduces degrees of freedom in H6 motion, and by W6.48, which undergoes a significant conformational change in response to agonist binding, associated with a change in the bend at P6.50. Consistent with early fluorescence spectroscopy studies on the β2-AR,[85] the conformational change in the extracellular half of H6, on going from the empty to the agonist-bound forms of TXA_2R, is properly marked by the shift of C257(6.47) from the membrane environment to the core of the seven-helix bundle (Figure 3). Consistent with structure comparisons of dark and photoactivated rhodopsin,[22] the agonist-induced active states inferred from this study are not associated with the dramatic detachment between H3 and H6 expected on the basis of early SDSL experiments on the photoreceptor in detergents.[25]

The communication between the two distal TXA_2R sites, i.e., the agonist-binding site and the cytosolic extensions of H3, H5 and H6, seems to be two-way and to require the integrity of the E/DRY arginine. In fact, the intramolecular communication occurs from the agonist binding site to the cytosolic domains, and, vice versa, from the neighborhoods of the E/DRY motif to the agonist binding site. In this respect, valine substitution for R3.50, in the cytosolic domains, is associated with a different configuration of the agonist binding site, compared to the WT^{U466} form, and with a different agonist-induced bend of H6 and conformational change of W6.48 (Figures 2 and 3).

The agonist-induced increase in solvent accessibility of the cytosolic extensions of H3, H5, and H6 is suggested to favor the docking of the C-terminal amino acids of the α5-helix of Gq_α in between H3 and H6. An important receptor recognition point in this respect is the arginine of the E/DRY motif that interacts with the C-terminal carboxylate and/or N351 of Gq_α (Figure 6).

Thus, the conserved arginine appears to be relevant for both the intramolecular communication between the agonist binding site and the G protein coupling domains of TXA_2R and the intermolecular communication between the TXA_2R and Gq. In this respect, the results of this study suggest that the R130V uncoupled TXA_2R mutant is impaired both in the ability to reach the proper configurations that characterize the active state ensembles and to recognize Gq via the highly conserved E/DRY motif.

The last 10 amino acids of Gq_α constitute the G protein portion that most penetrates the receptor. However, the results of this study suggest that, whereas the C-terminus of Gq_α seems to be the primary recognition point for the receptor, multiple Gq_α portions participate in the receptor−G protein interface. In fact, the α4/β6 loop recognizes the cytosolic extension of H6, whereas the α2−β4 and α3−β5 loops and the N-terminus of the β1-strand (or the C-terminus of the αN-helix) recognize H8 and the C-tail of the receptor (Figures 5 and 6). We speculate that the establishment of receptor−G protein contacts is instrumental in antagonizing the tendency of the C-terminus of the α5-helix to interact with the junction between αN-helix and β1-strand, in the receptor-free form of the G protein.

The formation of such a composite receptor−G protein interface is instrumental for activated receptor to induce concerted motions in β1/α1 loop, α1-helix, linker 1, αF-helix, switches I and II, β2-β3-hairpin, α2-helix, αG-helix, β6/α5 loop, and α5-helix. Consistent with experimental evidence,[30−32] the α5-helix of Gq_α appears to play the most relevant role in mediating receptor effects on the dynamics of the G protein. In fact, its motion influences directly the motion of the β6/α5 loop and, indirectly, i.e., via the β2-β3 hairpin, the motion of both switches I and II (Figures 7−10). The receptor-induced movements of these G protein portions are associated with an increase in the constitutive rotation of the α-helical domain with respect to the Ras-like domain, the bending points including switch I (Figures 7 and 12). An increase in solvent accessibility of GDP constitutes an additional feature of the receptor-bound states of Gq_α compared to the receptor-free ones. This effect is putatively associated with receptor-induced motions of the β1/α1 loop, and of the α1-, αF-, and αG-helices, which all participate in the nucleotide binding cleft. A putative GDP exit route is suggested to lie in between the αF and the β6/α5 loop, which undergo a significant detachment, on going from the free to the receptor-bound forms of Gq_α (Figure 10). This effect is also accounted for by the solvent exposure of amino acids in the α1- and αF-helices and in the β6/α5 loop (i.e., Q52, L174, and T326, respectively), marking the opening of a solvent-exposed crevice in the nucleotide binding site (Figure 10). The location of the putative GDP exit route, as predicted from this study, is consistent with the results of a very recent SDSL study.[33] Indeed, inferences from SDSL experiments hypothesize the formation of a GDP exit route following side-chain motions in the αF-helix and the α5/β6 loop.[33] Our results add more information, suggesting that the receptor-induced movements of these two G protein domains, which are associated with an increase in solvent exposure of GDP, involve both backbone and side chains. Intriguingly, the receptor-catalyzed motion of switch II

(82) Angelova, K.; Fanelli, F.; Puett, D. *J. Biol. Chem.* **2002**, *277*, 32202−13.
(83) Fanelli, F.; Verhoef-Post, M.; Timmerman, M.; Zeilemaker, A.; Martens, J. W.; Themmen, A. P. *Mol. Endocrinol.* **2004**, *18*, 1499−508.
(84) Vitale, R. M.; Pedone, C.; De Benedetti, P. G.; Fanelli, F. *Proteins* **2004**, *56*, 430−48.
(85) Gether, U.; Lin, S.; Ghanouni, P.; Ballesteros, J. A.; Weinstein, H.; Kobilka, B. K. *EMBO J.* **1997**, *16*, 6737−47.

and α2-helix away from the nucleotide binding site, as inferred from our computations, is similar to the one revealed by the structure of the KB-752 GEF peptide bound to Gi_α.[28] However, this consistency occurs despite a substantial disagreement concerning the putative GDP exit site. In fact, the complex between the GEF peptide and Gi_α seems to support the "lever-arm" model proposed by Bourne and co-workers, which would predict a GDP exit site at the $G_\alpha-G_\beta$ interface.[26−28] In contrast, our results suggest that such a receptor-catalyzed displacement of switch II and α2-helix is compatible with a different GDP exit route. This apparent inconsistency may be due to substantial differences between the binding modes of the KB-752 peptide and TXA_2R. Indeed, the latter is predicted to establish a remarkably more complex network of interactions with the G protein α-subunit compared to the KB-752 GEF peptide. Exemplar, in this respect, is the role of the C-terminus of the α5-helix as a fundamental G_α recognition point for the receptor but not for the KB-752 GEF peptide. These differences are suggestive of different mechanisms of nucleotide exchanges by the GPCR and the GEF peptide.

5. Summary

The results of this study provide insights into the mechanistic connection between intramolecular changes in a GPCR, as induced by an activating ligand, and structure and dynamics properties of a GDP-bound heterotrimeric G protein in response to receptor binding. The inferences from this study rely on extensive comparative analyses aimed at highlighting a few but significant structural features that mark differences among receptor and G-protein states. Two-way pathways mediate the communication between the receptor−G protein interface and both the agonist binding site of the receptor and the nucleotide binding site of the G protein.

Collectively, the increased solvent accessibility in the neighborhoods of the highly conserved E/DRY motif, shown by the agonist-bound forms compared to the empty receptor states, is instrumental in favoring the penetration of the C-terminus of Gq_α in between the cytosolic ends of H3, H5, and H6. The arginine of the E/DRY motif is an important mediator of the intramolecular and intermolecular communication involving the TXA_2R.

The receptor−G protein interface is predicted to involve multiple regions from the receptor and the G protein α-subunit, i.e., H3, H5, H6, H8, and the C-tail, from the receptor, and the C-terminus of the αN-helix/N-terminus of the β1-strand, the α2/β4, and α3/β5 and α4/β4 loops as well as the C-terminus of the α5-helix, from Gq_α. However, receptor contacts with the C-terminus of the α5-helix seem to be the major players in the receptor-catalyzed formation of a nucleotide exit route. In fact, the establishment of contacts between the receptor and the C-terminus of the α5-helix directly affects the motion of the β6/α5 loop and indirectly, i.e., via the β2-β3 hairpin, the motions of both switches I and II. In this respect, the receptor-induced pull of the β2/β3 turn by the α5-helix is suggested to (a) push switch II and the connected α2-helix toward the G_α-G_β interface, (b) straighten switch I and push up the connected αF-helix, and (c) detach the α1/β1 loop from both the C-terminus of switch I and the N-terminus of switch II. Linked to these motions, and also because of the establishment of contacts between the receptor and the junction between αN-helix and β1-strand, the β1-strand and the β1/α2 loop undergo a straightening that pushes up the α1-helix in between the αF-helix and the β6/α5-loop. As a consequence, the latter two portions undergo a separation, leading to the formation of a putative nucleotide exit route. Thus, the receptor-catalyzed nucleotide exchange is expected to involve the formation of an exit route in between the αF-helix and the β6/α5 loop. This structural change is concomitant with the interposition of the α1-helix in between the αF-helix and the β6/α5 loop, giving solvent accessibility to the anchored nucleotide. The mechanism of nucleotide exchange as catalyzed by a GPCR is expected to differ from the one triggered by the KB-752 GEF peptide.

The inferences from this study are of wide interest, as they are expected to apply to the whole rhodopsin family, also given the considerable G-protein promiscuity.

Acknowledgment. This study was supported by a Telethon-Italy grant no. S00068TELU (to F.F.).

Supporting Information Available: Additional analysis plots (Supporting Information Figures 1−4). This material is available free of charge via the Internet at http://pubs.acs.org.

JA077268B